

Tristan Reinisch

Optimization of a resonant photoacoustic cell for determination of soot mass concentrations

MASTER THESIS

For obtaining the academic degree
Diplom-Ingenieur

Master Programme of
Advanced Materials Science



Graz University of Technology

Supervisor:

Ao.Univ.-Prof. Dipl.-Ing. Dr.techn. Roland Resel
Institute of Solid State Physics

Graz, January 2013

Deutsche Fassung:
Beschluss der Curricula-Kommission für Bachelor-, Master- und Diplomstudien vom 10.11.2008
Genehmigung des Senates am 1.12.2008

EIDESSTÄTLICHE ERKLÄRUNG

Ich erkläre an Eides statt, dass ich die vorliegende Arbeit selbstständig verfasst, andere als die angegebenen Quellen/Hilfsmittel nicht benutzt, und die den benutzten Quellen wörtlich und inhaltlich entnommene Stellen als solche kenntlich gemacht habe.

Graz, am

.....
(Unterschrift)

Englische Fassung:

STATUTORY DECLARATION

I declare that I have authored this thesis independently, that I have not used other than the declared sources / resources, and that I have explicitly marked all material which has been quoted either literally or by content from the used sources.

.....
date

.....
(signature)

Ein ganz besonderer Dank geht an meine Frau Lisbeth und meine Tochter Lilly Sophie, die mich immer unterstützt haben und vor allem viel Geduld mit mir hatten.

Weiters möchte ich mich für die Betreuung durch Roland Resel an der Technischen Universität Graz und bei Alexander Bergmann in der AVL List GmbH bedanken. Weiters danke ich Robert Diewald und Klaus Harms für ihre kritischen Fragen, die ein rasches Weiterkommen ermöglicht haben und Bernhard Gaulhofer und Helmut Pongratz für die Unterstützung bei der Erstellung des Auswerteprogramms für den Betrieb des Versuchsaufbaus.

Abstract

The dust emission of combustion engines is a present health related issue. The classification of dust can be done mainly by determination of aerosol mass concentration. A very elegant way to probe the mass concentration is the so called photoacoustic principle. A major requirement for the photoacoustic sensor and its application in emission measurement is a sensitivity of about $1\mu\text{g}/\text{m}^3$. Due to the weak photoacoustic signal at low mass concentration the standard approach with a single cylindrical absorber and resonator cavity is no longer sufficient. Within the present work a special resonant system is developed which is built up by two cylindrical cavities in a T-shape. The acoustic signal is generated in the horizontal absorber tube and is further amplified in the vertical resonator tube. The optimum of the resonant signal is achieved by a 2:1 ratio of the absorber and the resonator lengths respectively. Further amplification of the resonant signal is realized by optimizing the diameter of the resonator tube. Numerical calculations of the Eigenfrequency spectrum on a resonant cavity system, where the cavity lengths are harmonized to a working frequency of the laser of 4000 Hz and a resonator diameter of 3 mm, has two resonances at 3200 Hz and 4500 Hz respectively. This cell geometry was verified experimentally and showed two significant peaks at similar frequencies in good agreement with the numerical calculations. By optimization of the resonator to 1.5 mm one significant resonance at 3900 Hz with a 2 to 2.5 time's higher amplitude arises due to an overlap of the two resonance frequencies. The overall gain in photoacoustic signal compared to the single cylindrical resonator is in the range of a factor of 2.5, leading to a significant improvement of the sensitivity.

Zusammenfassung

Die Luftverschmutzung durch Abgase von Verbrennungskraftmaschinen und die darin enthaltenen Nanopartikel oder besser bekannt als Feinstaub sind ein viel diskutiertes Problem und begegnen uns im täglichen Leben. Es gibt mehrere Möglichkeiten um Abgase zu klassifizieren. Eine davon ist die Bestimmung der Ruß-Massenkonzentration in Abgasen durch das photoakustische Messprinzip. Die Hauptanforderung an einen photoakustischen Sensor und seine Anwendung in der Emissionsmessung ist eine Sensitivität von $1\mu\text{g}/\text{m}^3$. Aufgrund des geringen photoakustischen Signals bei niedrigen Massenkonzentrationen ist die Verstärkung mit einem zylindrischen Resonator-Volumen nicht mehr ausreichend. In dieser Arbeit wurde ein spezielles Resonator-System entwickelt, welches durch zwei zylindrische Volumen in T-Anordnung realisiert wurde. Das im horizontalen Absorber erzeugte akustische Signal wird durch den senkrecht dazu angeordneten Resonator zusätzlich verstärkt. Das größte resonante Signal wird bei einem Verhältnis von 2:1 der Absorber- zu Resonator-Länge erzielt. Eine weitere Verstärkung des resonanten Signals wird durch die Optimierung des Resonator-Durchmessers erreicht. Numerische Berechnungen des Eigenfrequenzspektrums des resonanten Systems, indem die Volumina auf eine Arbeitsfrequenz des Lasers von 4000 Hz abgestimmt sind und der Resonatordurchmesser 3 mm beträgt, zeigen zwei Resonanzen bei 3200 Hz und 4500 Hz. Eine experimentelle Bestimmung des Eigenfrequenzspektrums der Zelle zeigt, in guter Übereinstimmung mit den Berechnungen, zwei Spitzen bei ähnlichen Frequenzen. Durch die Optimierung des Resonator-Durchmessers auf 1.5 mm entsteht eine markante Resonanz bei 3900 Hz mit 2- bis 2.5-mal höherer Amplitude, die durch die Überlappung der beiden Resonanzen zustande kommt. Die Intensität des photoakustischen Signals ist im Vergleich zu einem einfachen zylindrischen Resonator ungefähr um den Faktor 2.5 höher, was zu einer deutlichen Verbesserung der Sensitivität führt.

Contents

1	Introduction	8
1.1	Economic background	8
1.2	History of photoacoustic spectroscopy	10
2	Photoacoustic Principals	12
2.1	Irradiation of light	12
2.2	Absorption of light by particles in an aerosol	18
2.2.1	Soot formation in a combustion	18
2.2.2	Heat - Pressure - Sound	23
2.3	Acoustic	25
2.3.1	Oscillations in a Cylindrical Volume	25
3	Simulation	28
3.1	COMSOL	28
3.1.1	Set up a model in Comsol	29
3.2	Simulation of the Acoustic Cell	32
3.2.1	Finding the shape	32
3.3	Numerical calculation of a T-shaped resonator	38
3.3.1	Geometry	38
3.3.2	Physical properties	38
3.3.3	mesh	40
3.3.4	Results	42
3.3.5	Simulated geometries	46
4	Experimental evaluation of different cell designs	49
4.1	Conventional - Prototyping and Rapid - Prototyping	49
4.2	Setup	54
4.2.1	Data logging	56
4.3	Measurements	57
4.3.1	Variable T-Cell	60
4.3.2	Conclusion of measurements	68

5 Comparison of Simulation and Experiments **69**
5.1 Different cell dimensions and the impact on the acoustic 69

6 Conclusion **74**

1 Introduction

1.1 Economic background

The AVL List GmbH has developed several years ago a measuring system to determine the soot mass concentration in exhausts by the photoacoustic principal [10][11]. This system is called Micro Soot Sensor. With the photoacoustic principal it is possible to make transient measurements. The detection limit is at about $5 \mu\text{g}/\text{m}^3$ and the detection range goes from 0.01 to $50 \text{mg}/\text{m}^3$ which could be expanded by a pre-conditioning unit when sampling exhausts with high soot mass concentrations. The gas exchange time of the cell is at about 1 second. For the detection of the acoustic signal an electret microphone is used. The microphone is the limiting factor related to the operating temperature because it only works up to a temperature of 50°C . The Micro Soot Sensor is used for applications like the optimization of the combustion of diesel engines and the quantification of Diesel Particle Filters (DPF).

New engines and DPF's becoming better and better over the time and so a new device based on the photoacoustic principal should be developed. The requirements that the new device should fulfill are:

- The sensor should become more sensitive. The detection limit of the Micro Soot Sensor is at about $5 \mu\text{g}/\text{m}^3$. By a revision of the optic system, the resonant system, the type of microphone and the signal post processing system the detection limit should reach down to $1 \mu\text{g}/\text{m}^3$.
- For a better time resolution the gas exchange time has to become faster from a value of 1 second to 0.5 seconds. The gas flow through the measuring section is $2 \text{ l}/\text{min}$. It is not possible to use a higher flow rate for a faster response because the flow has to be strictly laminar. The smallest diameter in the gas path is 6 mm where higher flow rates could become turbulent.
- The dimensions of the device should become smaller so also the measuring chamber should have smaller dimensions. This has to be considered during a redesign of the resonant cavity system.

- The pollution of the measuring chamber by soot particles can influence the measurement. Deposited particles on the inlet and outlet windows of the laser will deliver a falsifying signal. Highly smooth surfaces and intelligent positioning of the windows can prevent the deposition of particles.
- The Micro Soot Sensor is heated during a measurement up to 50°C to prevent thermophoretic particle deposition and condensation of water in the cell. Thermophoretic particle deposition is caused by a temperature gradient in the gas. Particles in the aerosol are pushed by gas molecules with different kinetic energy in the temperature gradient. There is a force on the particles to move them to colder regions. The effect increases with the temperature gradient [26]. In a non heated measuring chamber the soot particles will be deposited on the walls which are colder than the sample gas. The used electret microphone is limiting the temperature of the system because it is not specified for higher temperatures than 50°C . With the usage of a T-shaped resonator the microphone is set on a position where it is possible to cool it. At higher temperatures of about 100°C pollution effects can be minimized because of a smaller temperature gradient between the sample gas and the cell walls. Further gaseous components do not condense as much as at 50°C .

1.2 History of photoacoustic spectroscopy

Alexander Graham Bell found the photoacoustic effect in an experiment with selen [1][2]. He excited selen by a monochromatic modulated light. At this time he had to split the natural light from the sun via prism to the spectral colors. He observed that the character of light has an effect to the illuminated material. At a specific wavelength the energy of the light was transferred to the specimen - it absorbs the light. A continuous light wave will result in continuous lattice vibrations and the material will be heated up. For the photoacoustic effect the incoming light is undulated to produce periodical lattice vibrations. This results in a cycle of heating and cooling of the material at the frequency of the undulated light. The thermal energy is also undulated transferred in an adiabatic process to the surrounding air from the surface of the specimen. A signal based on a modulated temperature gradient in the air can be measured as a pressure difference. An undulated pressure field is also known as an acoustic sound wave. This acoustic sound wave has the same frequency as the incoming light and could be detected, in the case of Bells setup, with a stethoscope or nowadays with a microphone.

This effect was found in gold, silver, platinum, iron, steel, brass, copper, zinc, lead, antimony, german-silver, Jenkin's metal, Babbit's metal, ivory, celluloid, gutta-percha, hard rubber, soft vulcanized rubber, paper, wood and glass [1]. At the beginning Bell didn't get results out of the experiments with carbon and thin microscope glass but in later experiments he did. Figure 1 shows the experimental setup of the photophone.

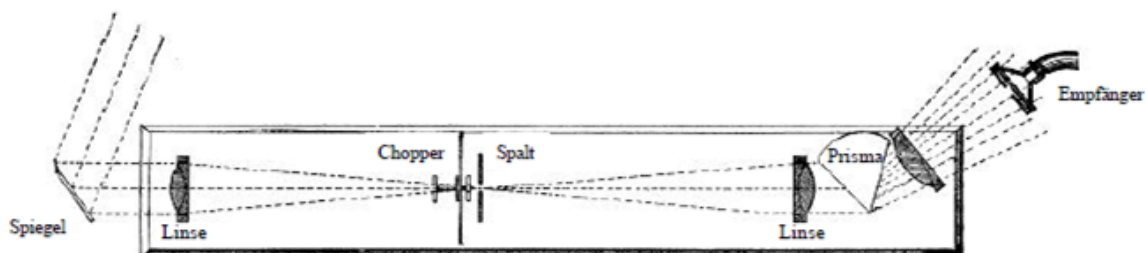


Figure 1: Experimental setup of the photophone of Alexander Graham Bell for the analysis of materials (e.g. selen) [1]. The light is irradiated over a mirror and a collecting lens, is modulated by a chopper wheel, collimated with a lens to split the light afterwards with a prism into the spectral colors and excite the specimen. The photoacoustic signal is detected by a stethoscope.

Alexander G. Bell saw it as a possibility to enhance the earlier developed electric telephone by the photoacoustic effect because no wires are necessary to transfer information over a distance. He named his invention the photophone regarding to the relationship of light and sound. In an experiment Bell could send spoken sentences over a distance of 213 meters.

The discovery of the photoacoustic effect was the basement for further inventions. In the year 1881 John Tyndall discovers the photoacoustic effect in gases [3]. During several years nothing happened on this scientific field until the year 1938 M.L. Viengerov was the first who used the effect for analytical detection of molecules in the gas phase. For the excitation of the specimen he used the light of an arc discharge of a carbon lamp and separated it with a prism [4]. The development of the laser in the year 1960 gave the possibility to use the monochromatic light for the excitation of to be analyzed materials. Kerr and Atwood [5] described in the year 1968 theoretical capabilities and experimental testing of pulsed ruby laser absorptivity spectrophone and a continuous wave CO_2 laser absorptivity spectrophone. In the year 1971 Kreuzer [6] used a He-Ne laser to measure the concentration of methane in nitrogen by the photoacoustic principle. An further development was to amplify the acoustic signal by the use of a resonator which was done by Dewey, Kamm and Hackett 1973 [7].

2 Photoacoustic Principals

The photoacoustic principal can be described in several steps, where each one outlines a separate chapter of physics starting at laser technology, over solid state physics and thermodynamics until acoustics. It can be described as a multiphysics principal.

2.1 Irradiation of light

Historically normal light from the sun or later special lamps were used for the excitation of the specimen. This light was modulated by a chopper wheel and afterwards split with a prism into the spectral colors. The absorption spectrum of a material defines which wavelength has to be used for a good photoacoustic signal. In a gas mixture like exhausts are a lot of components with different absorption spectra. To find a wavelength where only soot has an absorption maximum is very difficult [22]. That is necessary to prohibit falsifying acoustic signals from other components in the sample gas. If other components are excited, then the soot particles, the detected acoustic signal is no longer proportional to the soot mass concentration. A big task is to take any component of the emission matrix into account when selecting the wavelength.

The photoacoustic is theoretically linked to the absorption spectroscopy. While in the absorption spectroscopy the signal depends directly on the absorption process, the photoacoustic signal depends on the concentration of the analyt. The photoacoustic signal has a linear correlation to the irradiated light which is explained later in equation 13. The information of the absorption of light by a material is described by the law of Lambert - Beer which has an logarithmic dependency 1. The principal of absorption spectroscopy is sketched in figure 2.

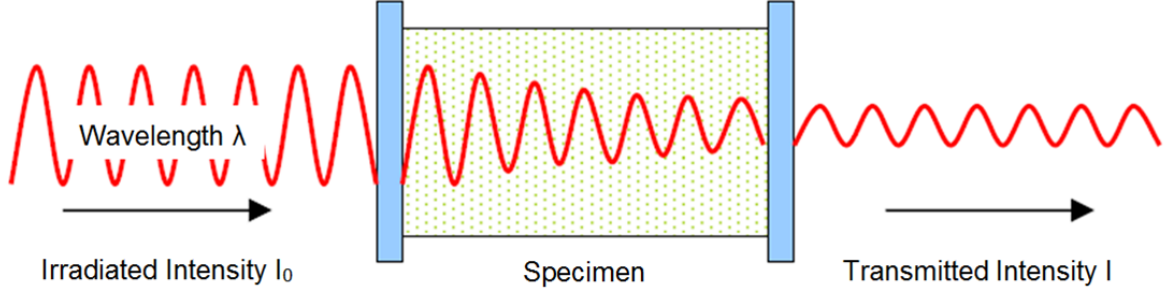


Figure 2: Principle sketch of absorption spectroscopy

$$A = \log \frac{I}{I_0} = \epsilon cd \quad (1)$$

In equation 1 A is the Absorption as a relation between irradiated light I_0 and transmitted light I and also as product of the wavelength dependent absorption coefficient ϵ , the concentration of the substance c and the path length d through the specimen.

Respectively the error propagation at the absorption spectroscopy has an exponential characteristic. Where the photoacoustic principle has the advantage of a linear characteristic and so the error propagation is also linear.

Nowadays the usage of lasers especially diode-lasers gave the possibility to irradiate monochromatic light. The output power of diode-lasers of several hundred milli-watts is high enough to generate an adequate acoustic signal of the analyt. The small scale of this type of lasers is sufficient for the usage in photoacoustic devices. Within the temperature stabilization by a Peltier-element or another adequate temperature stabilization, it is possible to adjust the diode-laser at a specific wavelength (e.g. at room temperature at 808 nm) and it could also be shifted over a small range of wavelengths. The shift is about 0.25 to 0.3 nm/K where the wavelength becomes longer at higher temperatures due to a reduction of the band gap in the semiconductor material in the laser. Depending on the laser-diode a shift of +- 5 nm can be performed. The frequency of the modulated light signal is harmonized to an Eigenfrequency of the resonator. The used signal shape is rectangular but it is also possible to use other types of shape [18] for the excitation like triangular, ramp or pulsed. The working principal of the irradiation is shown in figure 3.

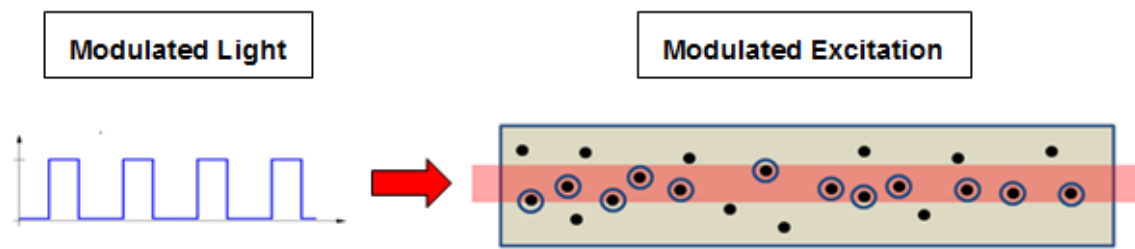


Figure 3: Modulated monochromatic light is irradiated into a resonant cell. Soot particles are excited by the light and dissipate the produced heat to the surrounding atmosphere. An acoustic signal is generated that is amplified by a resonator.

The laser beam is collimated by a lens-system in a way that the cross-section of the laser beam is nearly constant in the absorption section of the resonant cell. The diameter of the laser beam has to be smaller than the diameter of the absorption section to avoid any reflection of the beam at the wall as shown in 3. Furthermore deposited particles in the cell will be excited if the beam passes too close to the walls and will generate a constant falsifying signal.

In figure 4 an experimental setup of a photoacoustic measurement system is shown. The modulated monochromatic light (1) is collimated by a simple lens system. The light enters end escapes over windows (2) the measuring chamber. The upper shell of the measuring chamber is removed to make the beam path of the laser light visible in the cell (3).

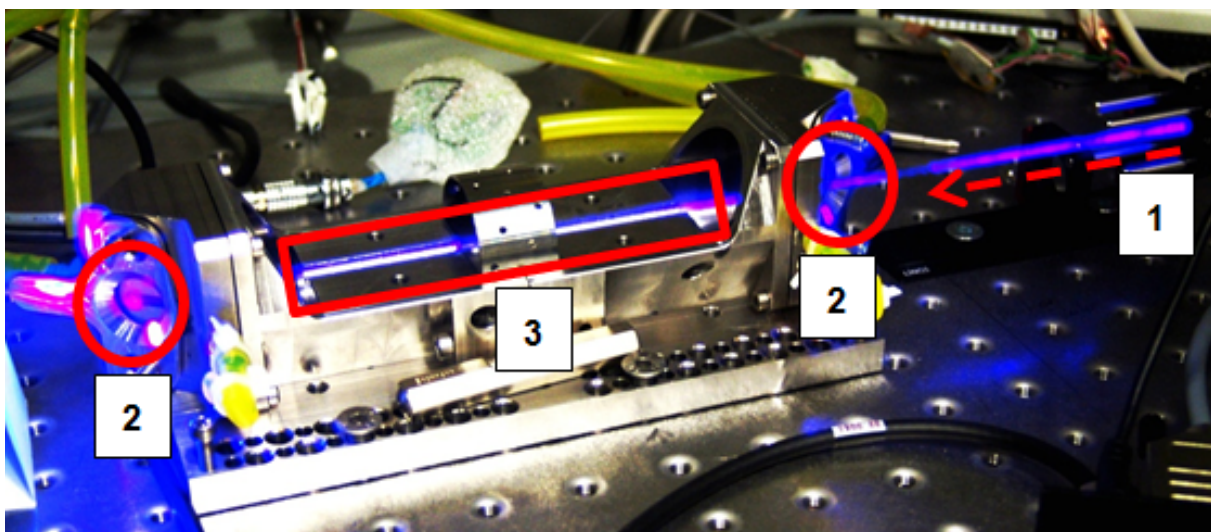


Figure 4: Experimental setup of a photoacoustic measurement system. The irradiation of monochromatic light and the beam path through a resonant cavity system is shown.

The sp^2 bindings of the graphite-like soot structure absorb light over a very broad wavelength range (UV to NIR) [27]. For the detection of the soot mass concentration, the wavelength has to be chosen carefully to minimize cross-sensitivities to other constituents [22]. The AVL's Micro Soot Sensor works at a wave length of 808 nm. In figure 5 the absorption cross-section of NO_2 is shown. NO_2 has a critical influence to the measurement of the soot mass concentration in exhausts. It is a fixed constituent of exhausts. The NO_2 concentration could be measured with other instruments and the photoacoustic signal could be corrected. Moreover a catalytic system could be used to reduce the NO_2 concentration in the aerosol.

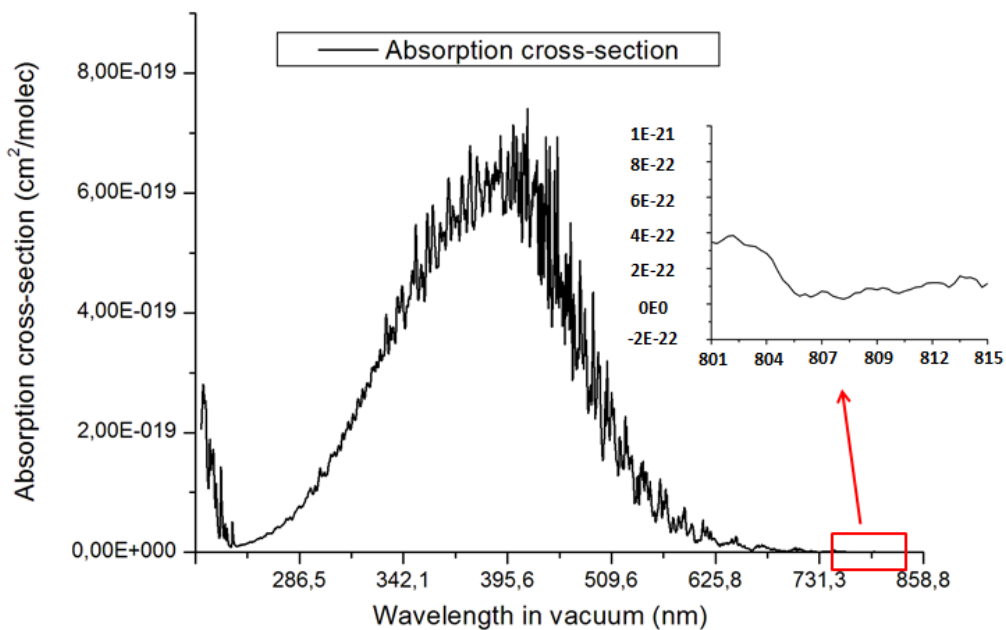


Figure 5: Absorption cross-section of NO_2 [8]

The magnified absorption cross-section of NO_2 in a range of 801 nm to 815 nm in figure 5 shows an enhanced absorption at about 802 nm. Figure 6 shows the photoacoustic signal of NO_2 sample gases in dependency of the wavelength. The local maximum at 804 nm matches to them of the reference spectrum [22]. At 808 nm the cross-sensitivity to NO_2 can be reduced to a minimum.

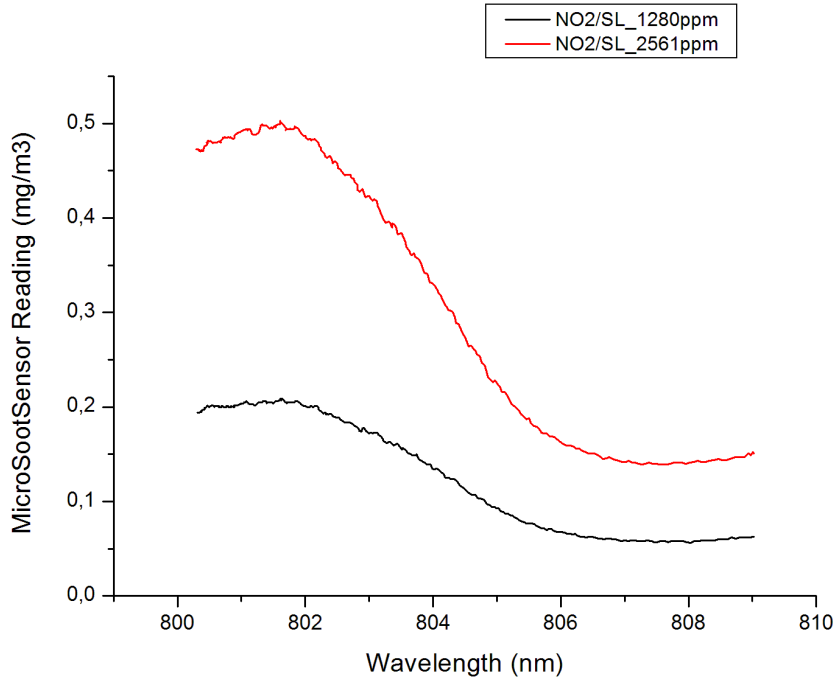


Figure 6: Photoacoustic signal NO_2 in dependency of the wavelength measured with a Micro Soot Sensor [22].

Figure 7 shows the infrared spectra of combustion generated soot at four different temperatures [27]. These spectra are examples for the transmission/absorption of light by soot. Because soot has different kinds of formation as explained in the following and so a general spectrum could not be used. In the spectra an local absorption maximum of CO_2 is marked at about $4.1 \mu m$ and the wavelength range where H_2O absorbs light is marked by the horizontal arrow. The other marked local absorption maxima starting at $7.94 \mu m$ up to $13.19 \mu m$ are special vibrations in graphite-like soot that are explained in detail in [27]. These absorption edges can not be detected with a photoacoustic system yet.

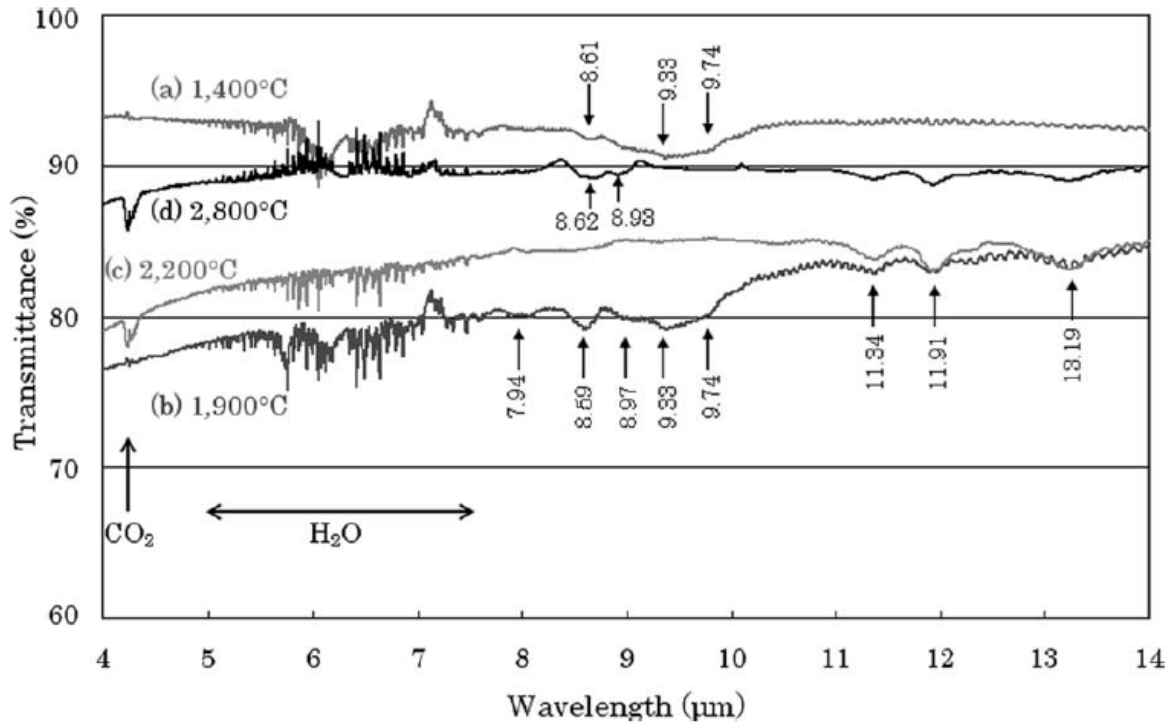


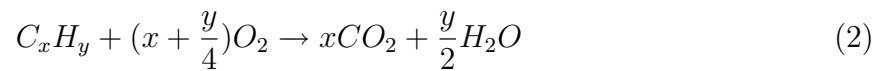
Figure 7: Infrared spectra of combustion generated soot at different temperatures. The figure shows local absorption maxima of soot, an absorption edge of CO_2 and a broad absorption region of H_2O [27].

2.2 Absorption of light by particles in an aerosol

A photoacoustic system is built to determine the concentration of an analyte in a matrix of other components. The photoacoustic signal is as good as the absorption of the analyte is. In this section the formation of soot particles and the absorption of light by soot particles is explained.

2.2.1 Soot formation in a combustion

The soot formation is a complex process of several steps. A complete combustion of hydrocarbons and oxygen can be written as



But a real combustion has never a complete reaction. Several side products like CO , H_2 , C_xH_y and at high temperatures and an oxygen overrun NO and NO_2 are formed. The basic module for the soot formation is Ethin C_2H_2 which is created in a low temperature combustion of about 2000 K and by the absence of oxygen. By additive reactions polyaromatic-hydrocarbons PAH are formed. If the PAHs have a spatial expansion it can be spoken about soot. The soot germ becomes bigger by coagulation and surface growing. The soot structure consists of crystal parts (graphite-like soot) where soluble parts are encased. The history of the formation process determines the content of the soluble parts. Young particles that are cooled down directly after the formation will have a big content of soluble parts. Otherwise particles which have a long stay time at high temperatures will have a higher content of crystal parts [17] [26]. For the photoacoustic effect the sp^2 bindings in the crystal structure is important. These bindings are responsible for the photoacoustic effect. Figure 8 shows the steps of the soot formation during the combustion process.

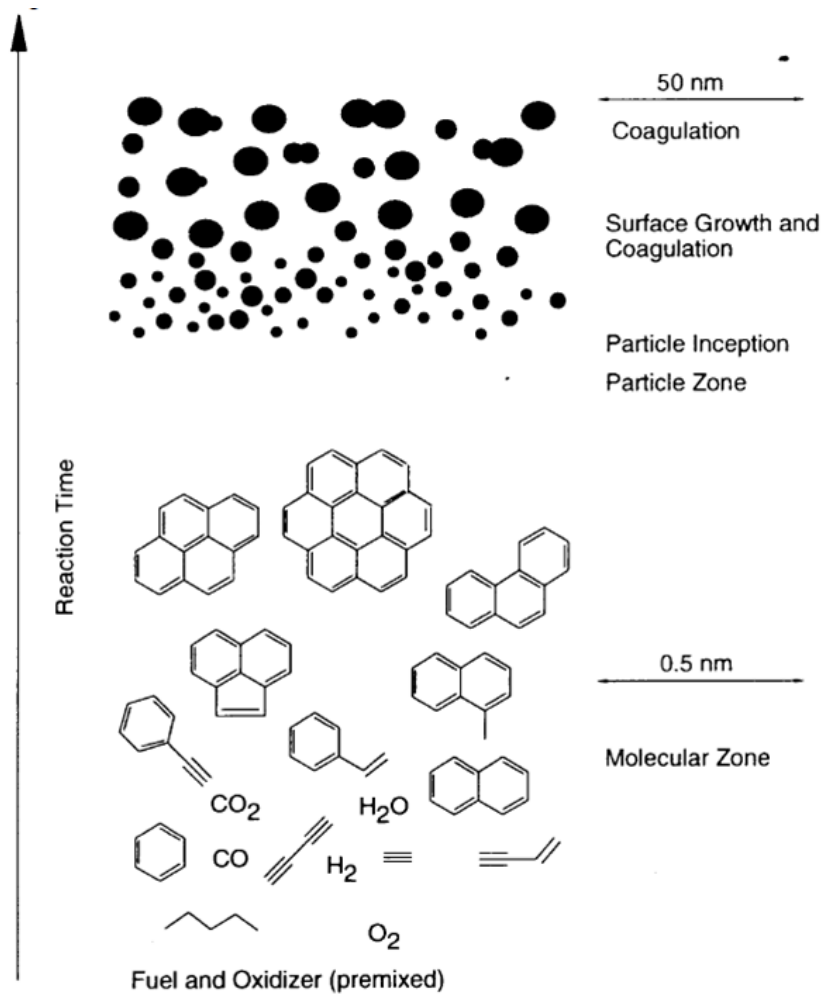


Figure 8: Formation of soot particles over the reaction time of a combustion [26].

The theoretical description uses simplified values for spherical particles. This description doesn't fit to the particles but to them of the primary particles. The problem could be handled with the following formulas. Never the less the photoacoustic systems is not as much sensitive enough to determine the origin of the signal or moreover if it comes from the primary particles or the particles itself. It is common to handle this argumentation with a reference diameter which characterizes a fractal by a spherical particle with an adequate diameter [21].

A soot particle is built up by primary particles with a diameter of 10 to 20 nm that can be seen in the figures 9 and 10. The primary particles have normally an almost amorphous structure constructed by graphene planes with a inter planar distance of about 2 to 3 nm [17] [19]. The amorphous structure could be seen in detail in figure 10.

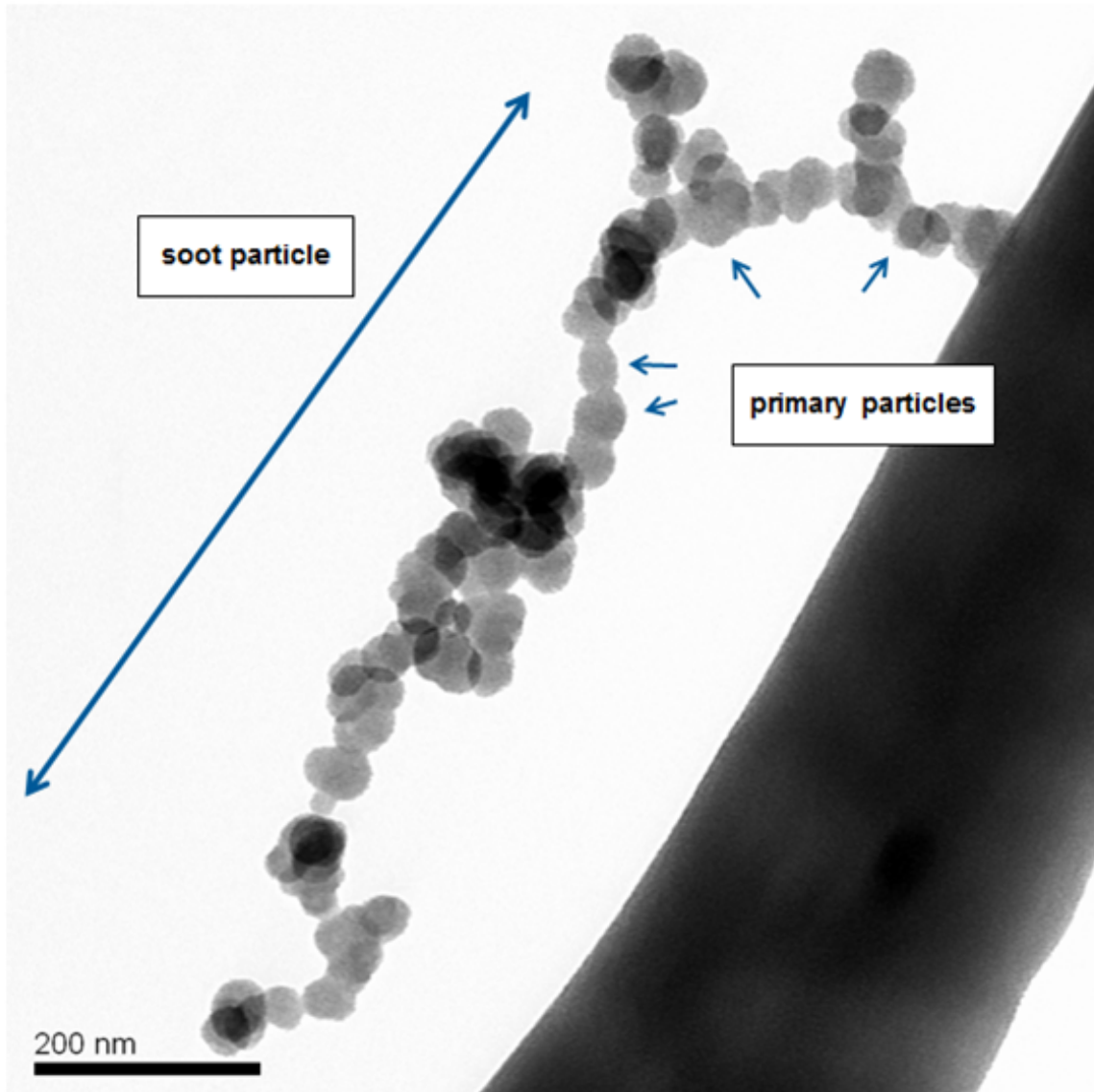


Figure 9: Picture of a Soot particle from a combustion generated aerosol taken with Transmission Electron Microscope (TEM). The soot particle sticks on a carbon substrate (broad black area on the right side of the picture).

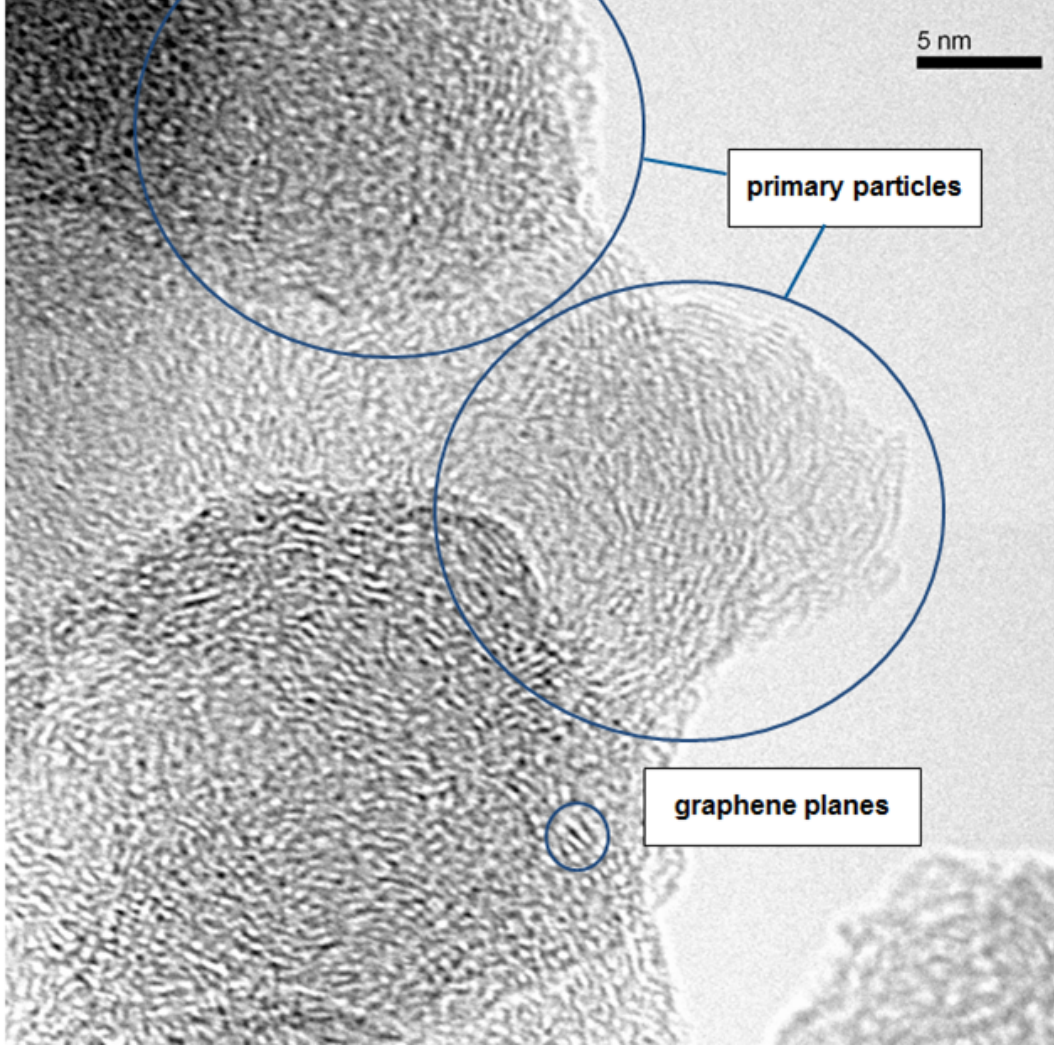


Figure 10: Picture of primary particles of a soot particle shown in figure 9 also taken with a transmission electron microscope (TEM). The primary particles could be characterized by their degree of graphitization [17] [19] [26].

For the description of the absorption process in particles some simplifications regarding the particle shape and the composition of an aerosol have to be done. The shape of a soot particle can be approximated by a spherical particle. The aerosol consists of a gas and levitating particles with different diameters [15]. The mass distribution $m(D_p)$ of particles in an aerosol is

$$m(D_p) = N * n(D_p) * \left[\frac{4}{3} \pi \left(\frac{D_p}{2} \right)^2 * \rho_p \right] \quad (3)$$

where the values are

- N ... particle number concentration
- D_p ... diameter D of spherical particles p
- $n(D_p)$... size distribution of particle diameter
- ρ_p ... density of particle

The mass related absorption cross section σ_{abs} of all particles in an aerosol is determined by the particle size distribution $n(D_p)$ and the absorption efficiency Q_{abs} which depends on the wavelength λ of the irradiated light.

$$\sigma_{abs} = \frac{\int_0^{\infty} \pi * \left(\frac{D_p}{2}\right)^2 * Q_{abs}(D_p) * N * n(D_p) dD_p}{\int_0^{\infty} m(D_p) dD_p} \quad (4)$$

The absorption coefficient α_{abs} at a defined wavelength λ and a fixed mass distribution $m(D_p)$ can be written as

$$\alpha_{abs} = \int_0^{\infty} \sigma_{abs}(D_p) m(D_p) dD_p \quad (5)$$

The mass concentration c_{mass} is defined by the integral of the mass distribution $m(D_p)$ over all particle diameters D_p .

$$c_{mass} = \int_0^{\infty} m(D_p) dD_p \quad (6)$$

Under the acceptance that the absorption efficiency Q_{abs} depends not on the particle diameter D_p , the absorption cross section of an aerosol is in the average constant and could be extracted from the integral. The simplified absorption coefficient α_{abs} is

$$\alpha_{abs} = \sigma_{abs} * c_{mass} \quad (7)$$

In a photoacoustic system all soot particles which are excited by the irradiated light will produce an acoustic signal. So the amplitude of this signal is proportional to the soot mass concentration c_{mass} . If the aerosol is sucked through a photoacoustic measurement system, changes of the concentration over the time could be detected by this principle. The correlation between acoustic pressure $p(r, t)$, the light intensity I_0 and the absorption coefficient α_{abs} is explained later in equation 13.

2.2.2 Heat - Pressure - Sound

The following summarized explanations of the theory of the formation of a sound wave by the photoacoustic principle could be looked up in detail at [7] and [13]. The energy absorbed by the particles depends further on the position and time related radiation intensity $I(r,t)$ and the absorption coefficient α_{abs} . The heat production can be written as

$$H(r, t) = \alpha_{abs} * I(r, t) \quad (8)$$

and acts on the assumption that the pressure in the measuring chamber is high enough to disregard radiating relaxations and wall collisions.

The periodical heating and cooling is generated by irradiated modulated light with one wavelength. The heat is transferred over the surface of the particle in an adiabatic process to the surrounding atmosphere. The following consideration is essential in conditional acceptance if the energy is completely converted to heat.

$$p(r, t) = P(r, t) - P_0 \quad (9)$$

The sound wave $p(r, t)$ is a position and time related pressure change that results from $H(r, t)$, $P(r, t)$ the entire Pressure and P_0 the mean pressure.

The inhomogeneous wave equation 10 is solved by Fourier Transformation. It is constituted by the series expansion of the eigenmodes of the homogeneous wave equation where c is the speed of sound, c_p is the specific heat capacity at constant pressure and β is the adiabatic volume expansion coefficient.

$$(\nabla^2 + \frac{1}{c^2} \frac{\partial^2}{\partial t^2})p(r, t) = \frac{\beta}{c_p} \frac{\partial}{\partial t} H(r, t) \quad (10)$$

The acoustic pressure produced by light absorption and heat transfer could be written as

$$p(r, t) = F^{-1} \left[\int_{r'} \frac{-\beta}{c_p} j\omega \tilde{H}(r', \omega) G_\omega(r|r') dr' \right] \quad (11)$$

The Green function $G_\omega(r|r')$ is defined by the geometry of the measuring chamber and boundary conditions. $\tilde{H}(r', \omega)$ is the Fourier transformed of $H(r, t)$. The heat production

could be split up in a time and a spatial dependent part.

$$H(r, t) = \alpha_{abs} I_0 R(r) M(t) \quad (12)$$

$M(t)$ describes the time dependency of I_0 . The shape of the signal can be rectangular, triangular or pulsed. For the experiments and the detection of the soot mass concentration a rectangular signal is used. The pulsed mode is actually not used in commercial systems because the available laser diodes do not fulfill the requirements for such a system especially the costs. $R(r)$ describes the spatial distribution of the laser beam and has a Gaussian shape. So the acoustic pressure is

$$p(r, t) = \alpha_{abs} I_0 \frac{\beta}{c_p} F^{-1} \left[j\omega \tilde{H}(\omega) \int_{r'} R(r) G_\omega(r|r') dr' \right] \quad (13)$$

with

$$F^{-1} \left[j\omega \tilde{H}(\omega) \int_{r'} R(r) G_\omega(r|r') dr' \right] = Z(r, t) \quad (14)$$

$$p(r, t) = \alpha_{abs} I_0 \frac{\beta}{c_p} * Z(r, t) \quad (15)$$

$Z(r, t)$ is the cell constant and describes the complete measurement setup and takes the beam profile and the shape of the signal into account.

2.3 Acoustic

The excited soot particles in the photoacoustic system can be perceived as point sound sources. These point sources will emit the sound wave in form of spherical waves. The fundamentals for that are described in detail in adequate literature (e.g. [13] and [14]).

2.3.1 Oscillations in a Cylindrical Volume

To enhance the acoustic signal from the analyzed material a resonator can be used to amplify the signal [7]. If the frequency of the modulated excitation matches to the cell dimension the sound waves which are produced by the analyt will interfere constructive and will form a standing wave. The higher signal intensity during the optimization of the shape of the resonator was the main goal of this thesis [7].

In a cylindrical cell three different resonances occur:

- An oscillation along the cylinder axis is determined as longitudinal resonance.
- An oscillation along the cylindrical shell is determined as azimuthal resonance.
- An oscillation along the radius of a cylinder is determined as radial resonance.

longitudinal - azimuthal - radial

Figure 11 shows the different pressure fields of the different resonances of a cylindrical both ends open pipe. The new resonator should be optimized to a longitudinal oscillation. This type delivers the highest acoustic pressure in a cylindrical volume and is more over understood at best of them.

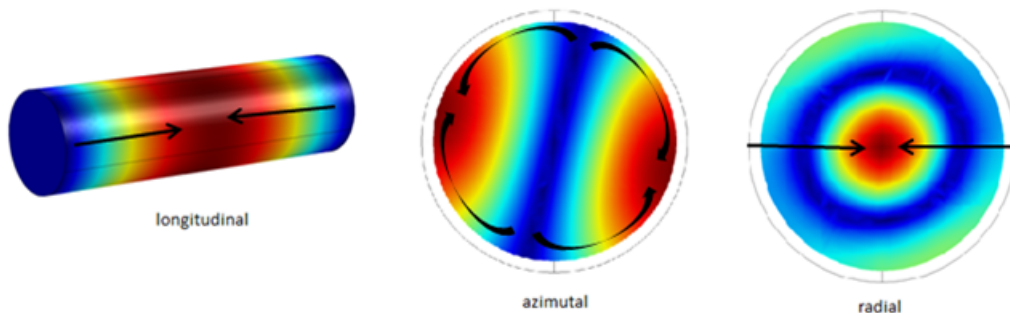


Figure 11: Pressure field of longitudinal, azimuthal and radial oscillations. The arrows show from fields of low pressure to fields of high pressure.

A both ends open cylinder is a resonator for sound waves that could be stimulated for self-oscillations. The waveguide cut-off frequency for longitudinal oscillations is the value $kR = 1.84$ where $k = \frac{\omega}{c}$ is the wavenumber and R the radius of the cylinder.

The value of 1.84 is defined over the root of the Bessel-function of the self-oscillations in a cylindrical volume. For a cylindrical resonator with a diameter of 6 mm the value is 0,221 at a frequency of 4000 Hz.

Due to that in this resonator can only occur longitudinal oscillations in a frequency range of several hundreds Hertz around the used working frequency of 4000 Hz. The three dimensional acoustic problem could be simplified to a one dimensional one because only the propagation along the x-axis is relevant [13].

$$\bar{p}(x) = (p_+ e^{jkx} + p_- e^{-jkx}) \quad (16)$$

The produced acoustic sound waves of the soot particles will propagate in radial symmetric directions. The diameter of the cylinder is much smaller than the length of the cylinder so the propagation direction only in positive or negative x-direction is relevant for the interference of the sound waves. All particles in the absorber are excited with the speed of light and so all elementary sound waves have the same phase. The one dimensional wave propagation is shown in figure 12.

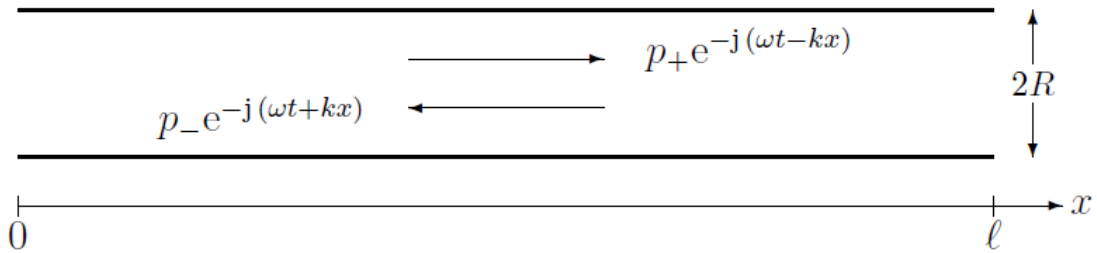


Figure 12: Directions of propagation of a sound wave in a cylindrical resonator in a one dimensional view [13].

A pressure wave that is propagating in the cylinder will be reflected at an open end with the opposite phase and at a closed end with the same phase. Through multiple reflections a standing wave is built up. For a both ends open cylinder the equation 17 and for a one side closed cylinder the equation 18 can be obtained.

$$f_n = n * \frac{c}{2L} \quad (17)$$

$$n=1,2,3,4,5\dots$$

$$f_m = m * \frac{c}{4L} \quad (18)$$

$$m=1,3,5,7\dots$$

For both equations L is the length of the cylinder and c is the speed of sound at a constant temperature. The values n and m characterize the mode of the oscillation. The one dimensional handling of that problem neglects the reflection of the sound waves at the inner walls of the cylinder. The propagation directions where the walls influence the sound wave are not considered. The walls are only taken into account at a two or three dimensional view of the problem.

3 Simulation

Numerical calculations of technical problems are common techniques to solve them fast and cost efficient. Here the problem was to find a way to simulate the resulting acoustic pressure of the photoacoustic signal at the position of the microphone in the resonant cell. The first step was to find the right software because there are not so many possibilities to simulate acoustic problems in three dimensions.

3.1 COMSOL

For the numerical calculations the commercial program *COMSOL Multiphysics* was used. This program is based on the finite element method. It has various possibilities to simulate different kinds of physical and chemical problems which are based on differential equations. For the problem the *pressure acoustic module* was used to determine on the one hand Eigenfrequency spectra of different cell geometries and on the other hand the resulting pressure of the photoacoustic signal at the position of the microphone.

To find numerical solutions of a real problem it has to be simplified often because it would need a lot of capacities and time to include all physical effects in one calculation. For the simplification the following physical phenomena are not considered in the calculations:

- Photoacoustic effect as its entirety - The irradiation of the modulated, monochromatic light, and the light absorption by the soot particles and the therefrom resulting acoustic sound waves.
- The gas flow through the cell with respect to a change of the ambient pressure due to pressure pulses caused by the sampling system.
- Surface and volume losses of the acoustic wave in the cell [12].

To simulate each of these problems close to the reality would demand a lot of time. The simplifications and boundary conditions will focus on the parameters which have the lowest influences on the behavior of the resonator.

The aim is to maximize the acoustic pressure of the photoacoustic signal at the position of the microphone. This can be realized by an optimization of the shape of the resonant measuring cell. With an special arrangement of two cylindrical tubes in a T-shape the

acoustic pressure could be amplified. To find the Eigenfrequency spectra of different cell geometries it is necessary to simulate the whole geometry. Small variations of the shape could have big influence on the spectrum and the resulting pressure.

3.1.1 Set up a model in Comsol

At the beginning the user has to choose the *Model Wizard* which space dimension the geometry should have. In figure 13 the user interface is shown. To reach short solving times, symmetries in the geometry could settle down the space dimension.

In the next step the physics which should be simulated has to be selected shown in figure 14. COMSOL has in the basic version most of the common used physics for simulations with the finite element method like AC/DC, Acoustics, Chemical Species Transport, Fluid Flow (also known as Computational Fluid Dynamics CFD), Heat Transfer, Structural Mechanics and a tool to implement your own physics in the Mathematics module. For more complex models additional packages are available. The next step is to choose the kind of study as shown in figure 15. In this pre-processing step of the calculation, the user could choose several kinds of study types like Eigenfrequency, Frequency Domain, Time Dependent, Stationary and others which are fitting to the study type.

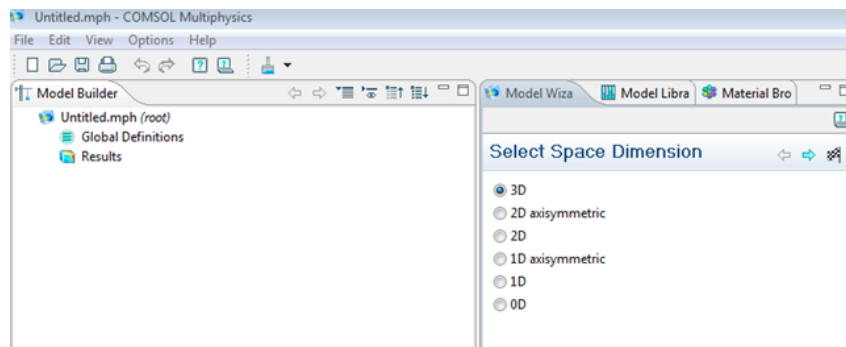


Figure 13: User interface for selecting *Space Dimension*

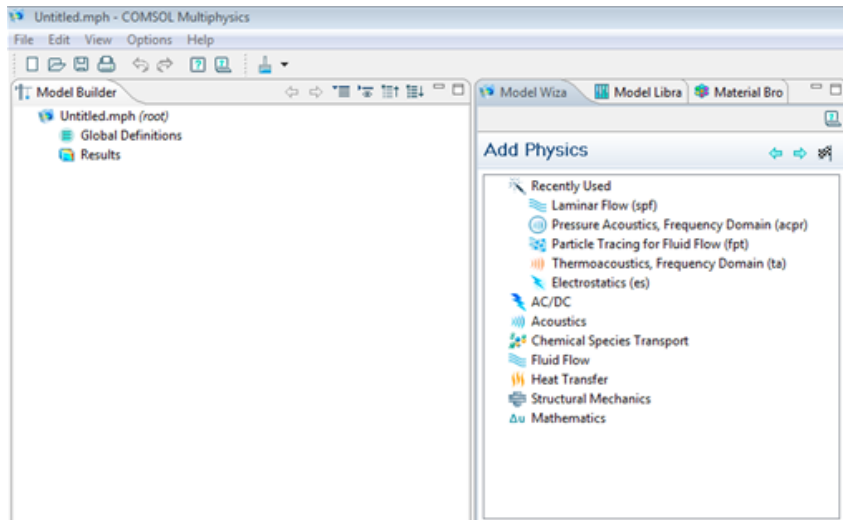


Figure 14: User interface for selecting *Physics*

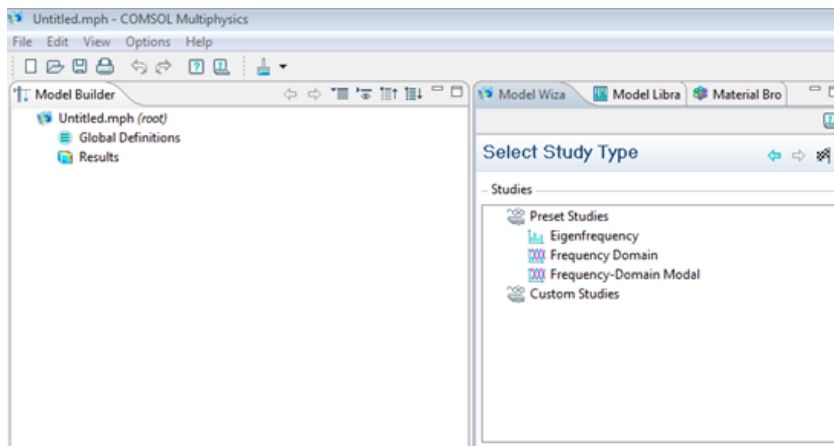


Figure 15: User interface for selecting *Study*

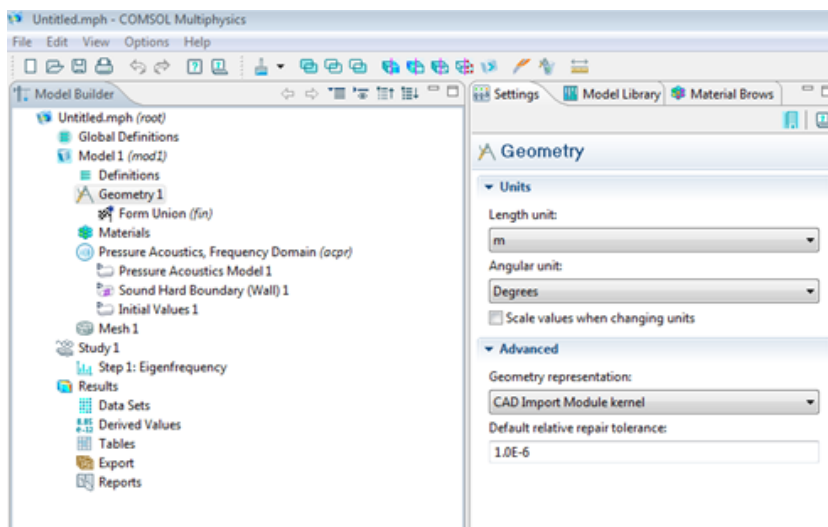


Figure 16: User interface of *Model Builder*

As shown in figure 16 the user has to work through the model builder. At the point *Global Definitions* common used parameters could be predefined to use shortcuts in the further process. The *Model configuration* includes the core of the physical problem. Geometries can be imported or can be drawn by yourself. The drawing tool includes only simple geometries and can not replace a professional drawing tool. At the point *Materials* the material properties are selected. The materials in this library are stored with known physical properties (e.g. speed of sound, heat capacity, density and so on). Any of these material properties has default values. Also own materials could be defined as well. Therefore it is necessary to know which properties are used by the predefined physics.

At the point *Physics* the user has to define the characteristics of the model. Initial values, boundary conditions and so on have also default values as the materials. For example, the pressure in a geometry which consists of air is set automatically to 1 [atm] and the temperature to 293.15 [K] which is the common used value of the room temperature. It is always possible to change the values of the material properties. The default settings should give the possibility to get quick results without handling details of the finite element method.

The next step is to set up a mesh on the model. At this point I want to refer to special literature because the step of meshing is a kind of art [24] [25]. One principle has to be considered always: as fine as possible - as coarse as necessary

As described before the point *Study* characterizes the problem. With the solver configurations a special solver could be set up and dependent variables could be configured. Further parameters and cluster computing could be distributed at this point [24]. The calculation can be started with the button *Compute* in the *Model Wizard*. Depending on the to be simulated problem and the number of finite elements the solution time varies. Certainly the used computer hardware pretends also the solution time. A concrete example is given later. Is the problem solved the post-process can start. COMSOL gives a broad range of possibilities to create graphics and graphs. Any solved parameters of the study could be plotted and exported. If the study includes several steps (time dependent solution, more than one eigenfrequency) also movies and animations can be created.

In the following it is explained which kind of geometries, material, physics are used to enhance the resulting pressure in the photoacoustic resonator at the position of the microphone.

3.2 Simulation of the Acoustic Cell

3.2.1 Finding the shape

The flow of the aerosol has to be adapt to the dimensions of the cylindrical pipe to prevent turbulences which can occur noises. Turbulences can be prevented by keeping the Reynolds number low. It is a dimensionless number which characterizes the flow of a fluid in a body. A fluid has the same flow properties in different bodies if the Reynolds number is equal.

The Reynolds number at a specific flow speed of a fluid in a cylindrical pipe is defined as:

$$Re = \frac{U \cdot d}{\nu} \quad (19)$$

$$U = \frac{\dot{V}}{A} \quad (20)$$

U... flow speed

ν ... viscosity of the fluid

\dot{V} ... Volume flow

d... diameter

A ... cross-section area (e.g. cylinder)

For a fast gas exchange time smaller diameters of the cylindrical cavities are better. Based on the experiences of the development of the AVL's Micro Soot Sensor three main parameters have to be considered during the redesign of the resonant cell:

- Acoustic Path - The geometry of the resonant system determines which acoustic resonances occur. The acoustic standing wave is built up in a system of different cylindrical volumes.
- Gas Path - For a fast responsible behavior the way of the aerosol through the cell has to be taken into account. A laminar flow of the aerosol is a requested to prevent an acoustic noise through turbulences.
- Laser Path - A straight alignment of the cylindrical volumes is necessary to avoid reflections at the cell walls. Therefore the laser beam is collimated and has a smaller diameter then the cylinders in the cell.

The Acoustic Path is the dominant one. Any change of the other ones has a direct impact to the standing acoustic wave. At first it should be described why the main geometry looks like a dumbbell as shown in figure 17. The measuring chamber has to be closed to the surrounding atmosphere otherwise the measuring of an aerosol does not make sense.

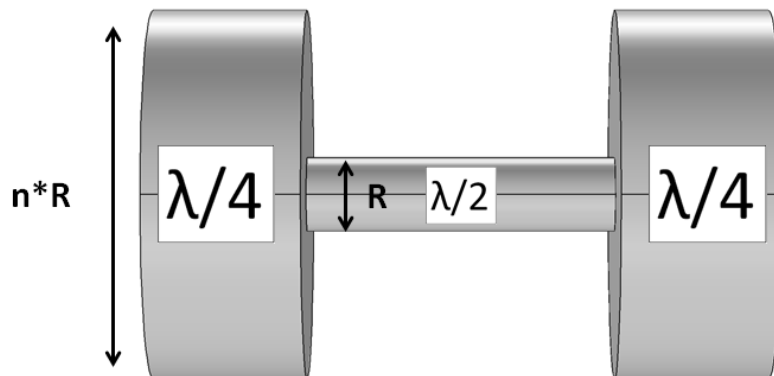


Figure 17: Both ends open resonator limited by two volumes. These volumes simulate the endless room where a propagating sound wave in the resonator is reflected.

So the resonator in figure 17 in the middle do not have the endless volume at both ends of the pipe which is necessary that a standing wave can be built up. The extension of the cross-section of this pipe to a multiple of the radius as it is shown in figure 17 is enough that the acoustic standing wave can be generated. The jump from a small diameter to a large diameter can be explained by the pressure which is the force of the acoustic sound wave, propagating in x-direction, acting against an area. In the absorber this area is small. At the crossover the force acts immediately on a much bigger surface. This causes a reflection of the sound wave with the opposite phase. The length of the resonator has to be calculated as shown in equation 21 for a both ends opened pipe which depends on the frequency and the speed of sound. Furthermore the lengths of both volumes which are simulating an endless room are also related to the values of the frequency and the speed of sound else than intended to the beginning of this work. If the resonator was designed for

the ground oscillation, than each cylindrical volume on the sides of the resonator should be as long as a quarter of the acoustic standing wave. These two volumes have a further function which name is giving to them - Notch-Filter. Noises with a specific frequency are filtered by these volumes and can not pass them. So signals which are not produced inside the resonator can not falsify the photoacoustic signal.

At the AVL's Micro Soot Sensor at the end of the Notch-Filters are the windows situated where the laser light can enter and leave the cell. If there are deposits on them which could absorb the light, noise is generated which can disturb the measurement of the analyte.

As explained before in a cylindrical both ends open volume different resonances occur. This resonator is constructed for longitudinal oscillations at a specific working frequency along the axis.

Bases on the acoustic fundamentals and the symmetry criteria of the length of the cavities it was time to let some new ideas in.

Most of the microphones are not use able at temperatures of 100°C as planned for the chamber. Therefore it is possible to displace it from the main gas-path to the end of a cylindrical resonator which should transport the acoustic signal from the absorber. This kind of shape is also known as "Helmholtz-Resonators" [20]. Simulations on different sizes of the length of this tube have been done by Baumann [12]. He declared the horizontal tube as the absorbing part of the photoacoustic system and the vertical one as the resonator. His resonator was acoustical isolated from the absorbing part by a diminution like the idea of Helmholtz. This gives the possibility to fix the longitudinal oscillation in the resonator at one frequency by a variation of the absorber dimensions.

The developed T-cell has no diminution at the changeover from the absorbing part to the vertical mounted tube. Instead of that a trumpet like shape should transport the acoustic pressure produced by the photoacoustic effect to the position of the microphone. In such a configuration there will occur two longitudinal oscillations which are termed in the following as the first and second Eigenfrequency of the system. These two resonances are a result of the coupled tube system. In a typical cylindrical resonator are the length and the diameter the only determining values for the frequency of longitudinal, azimuthal and radial resonances. In a T-shaped cell are more values which have an influence on the position and the resulting acoustic pressure as well:

- In the horizontal tube the soot particles are excited - so the length and the diameter of it, determine how many particles are in the absorbing section. In that point of view the dimension of the laser beam has almost the same size as the tube.
- In the vertical tube is no excitation of the soot particles - the produced acoustic pressure is dispersed by its volume (diameter, length).
- The ratios of the values of horizontal and vertical tube will determine the position of the first and second Eigenfrequency.

All these values have to be considered during the optimization process.

The resonant cell has to be optimized to a frequency of about 4000 Hz. The new soot sensor will be used in the automotive branch where disturbing noises (e.g. turbo charger) occur beneath the 4000 Hz. The length of a cylindrical resonator with both ends open is defined as

$$L = \frac{n}{2} \cdot \frac{c}{f} \quad (21)$$

L . . . length of the both ends open cylinder

n . . . harmonics

c . . . speed of sound

f . . . frequency

The length of such a resonator is reciprocal to the excitation frequency. So a compromise is needed between a longer excitation zone and the frequency. A longer absorbing section cause a higher acoustic signal at low frequencies and vice versa. The 4000 Hz are also used at the in use device. The length of the resonator is long enough to generate a use able acoustic signal. Figure 18 shows the volume of a T-shaped cell where the absorbing section is located between two volumes which are simulating the endless room and are necessary that a standing wave can be built up.

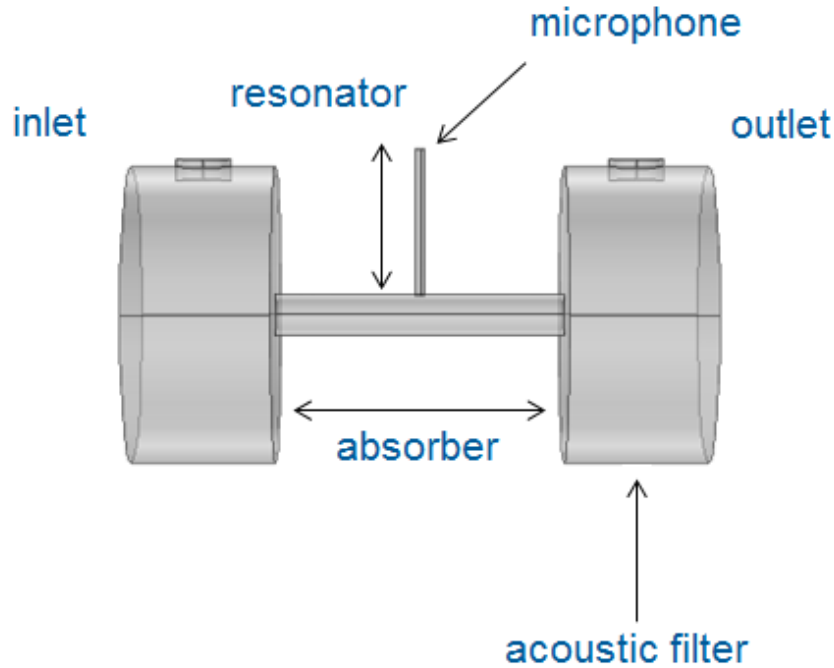


Figure 18: Terms of a T-shaped cell

The diameter of the absorbing section needs also a compromise similar to them above. The tube should be small enough that no azimuthal or radial resonances occur in the specific frequency range and further the gas change time can be low. But on the other hand the flow has to be laminar where a small diameter is limiting. The flow behavior as described before is characterized by the Reynold's number. At a flow of 2 l/min through the cell the Reynold's number is 475 at an air temperature of 20°C with the dynamic viscosity of air of $1.49 \cdot 10^{-5} \text{ m}^2/\text{s}$. A critical value where a flow of hot exhausts becomes turbulent is 1500.

A further request is that the microphone shouldn't be exposed to the exhaust flow as in the Micro Soot Sensor. The position is now at the end of the resonator. That gives the possibility to cool the microphone without an influence on the exhaust.

For the simulation and also the experiments several cell-dimensions have been analyzed. Therefore it was necessary to name each cell regarding to the dimensions. In the following the different cells are named as shown in figure 19 which shows a T-shaped resonator that is optimized to a working frequency of about 4000 Hz and the speed of sound in air at room temperature. The diameter of the absorber is always 6 mm and the lengths of the notch filters are always 21 mm with a diameter of 43 mm.

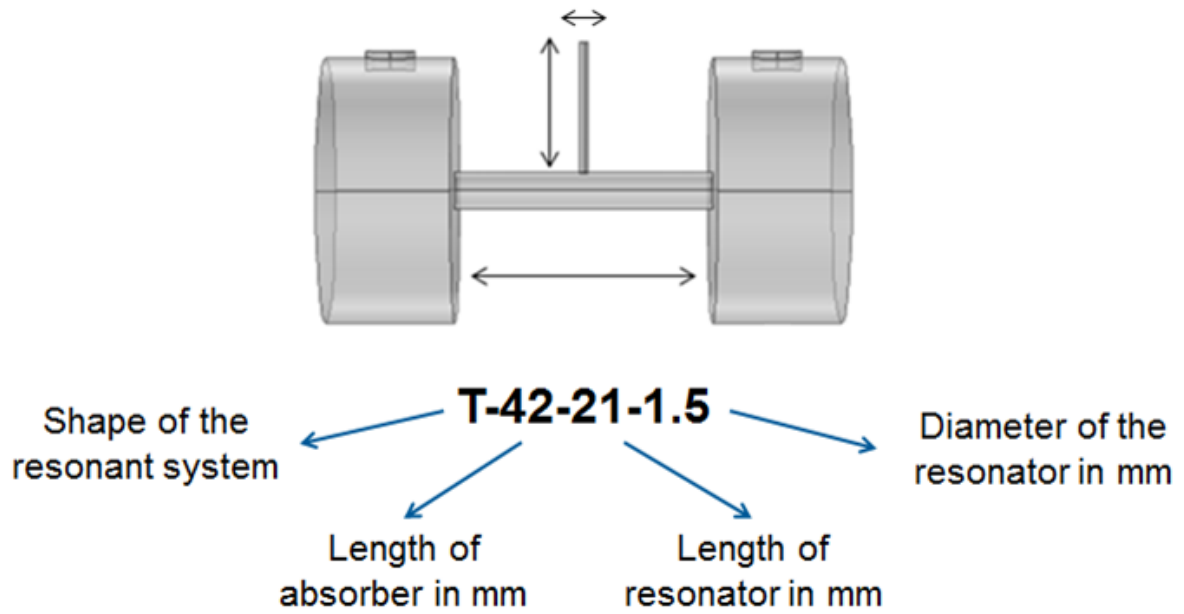


Figure 19: Nomenclature of a resonator system with the the characterizing values the length of the absorber, the length of the resonator and the diameter of the resonator.

3.3 Numerical calculation of a T-shaped resonator

For this thesis the Eigenfrequencies of a photoacoustic resonator have been analyzed. The Eigenfrequencies are calculated by the partial differential wave equation shown in 24.

3.3.1 Geometry

In the following the calculation and results of a T-shaped resonator are explained where the dimensions of it are tuned to a working frequency of about 4000 Hz, is named T-42-21-15 and is shown in figure 18 and 19. The geometry has three dimensions and can be separated into six different domains which are the inlet, the outlet, the left and right Notch-Filter, the absorber and the resonator. The domains are limited by 54 boundaries and they are further limited by 110 edges. The used unit for the lengths is millimeter and the angles are specified with the unit degree.

3.3.2 Physical properties

The material of the domains is air. For the calculation of the acoustic behaviors the density of the material and the speed of sound in the material have to be known. The correlations of both values and others are:

$$\rho = \frac{p}{R_S * T} \quad (22)$$

The Density ρ is given by the air pressure p which is set in all calculations to 1 atm, the specific gas constant R_S (dry air $R_S = 287.085 \frac{J}{kg * K}$) and the temperature T with 298.15 K.

$$c_s = \sqrt{\kappa * \frac{p}{\rho}} \quad (23)$$

For the speed of sound c_s in dry air at a temperature of 298.15 K the adiabatic index κ is 1.402. For the same value for p as above is $c_s = 343m/s$.

The *Acoustic module - Eigenfrequency* of COMSOL uses the inhomogeneous Helmholtz equation 24 to solve acoustic eigenvalue and eigenfrequency problems [24].

$$\nabla * \left(-\frac{1}{\rho}\right)(\nabla p - \vec{q}) - \frac{\omega^2 p}{\rho c^2} = Q \quad (24)$$

- ρ ... Density of material
- p ... acoustic pressure with $p = p(\vec{x}, \omega)$
- ω ... angular frequency
- c ... speed of sound in material
- q ... term of dipole source
- Q ... term of monopole source

For a study of the eigenfrequency of a domain the terms of the monopole and dipole source are zero and the equation is simplified to

$$\nabla * \left(-\frac{1}{\rho}\nabla p\right) + \frac{\lambda^2 p}{\rho c^2} = 0 \quad (25)$$

λ is the eigenvalue and is related to the eigenfrequency f and the angular frequency ω through

$$\lambda = j2\pi f = j\omega \quad (26)$$

The walls of the cell are defined as sound hard boundaries, which are boundaries at which the normal component is zero. That means that the wall does not interact with the sound waves and reflect them. The boundary condition for a sound hard boundary is

$$-\vec{n} * \left(-\frac{1}{\rho_0}(\nabla p - \vec{q})\right) = 0 \quad (27)$$

The inlet and outlet for the sample gas in the cell are positioned at the upper ends of the Notch-filters as shown in figure 20. The high lighted surfaces are defined as sound soft boundaries. That means that the acoustic pressure vanishes there. This is an approximation for a tube system that is connected to the cell to transport the sample gas. The boundary condition for a sound soft boundary is

$$p = 0 \quad (28)$$

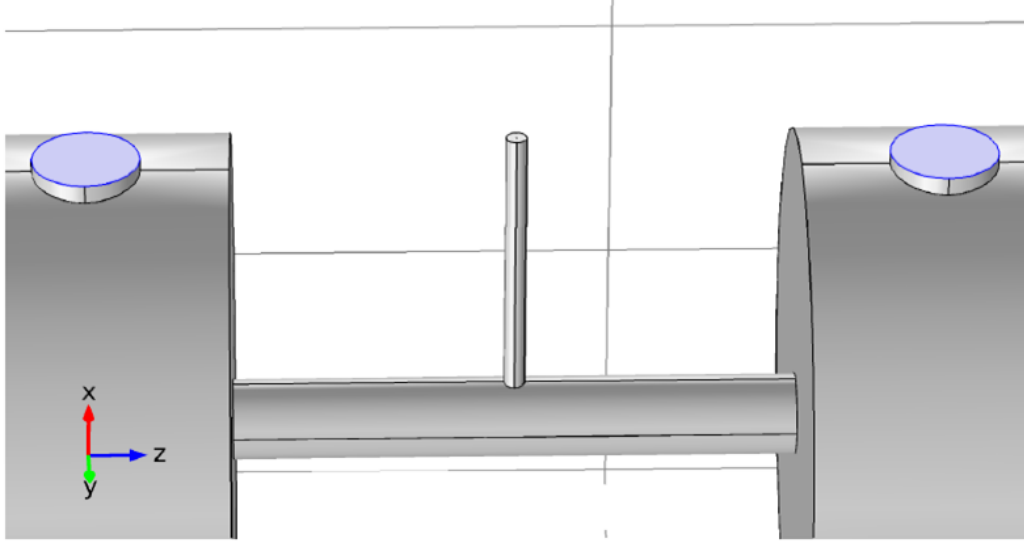


Figure 20: In- and outlet of the cell (blue) are defined as sound soft boundaries

3.3.3 mesh

As said before meshing is the most important thing for a calculation of finite elements. The length of a period of a sound wave has to match to the size of the finite elements. For the calculation the maximum element size h_{max} is limited by the speed of sound c and the frequency f as shown in equation 29. The maximum element size of a finite element is defined by its geometry e.g. the characteristic value for a cube is the space diagonal. For this study a frequency range up to 8000 Hz is relevant because the geometry is optimized to a working frequency of about 4000 Hz. The results have an adequate numerical accuracy for that frequency range.

$$h_{max} < 0.2 \frac{c}{f} \quad (29)$$

For a speed of sound in air c at room temperature and a frequency f of 8000 Hz the maximum element size is $h_{max} = 8.5mm$.

The following table 1 shows the settings for the mesh elements and figure 21 shows the meshed geometry.

Table 1: Settings for finite elements of T-42-21-1.5

Name	Value	Property	Value
Maximum element size	8.4 [mm]	Tetrahedral elements	7531
Minimum element size	1.51 [mm]	Triangular elements	2268
Resolution of curvature	0.6 [mm]	Edge elements	458
Resolution of narrow regions	0.5 [mm]	Vertex elements	68
Maximum element growth rate	1.5		

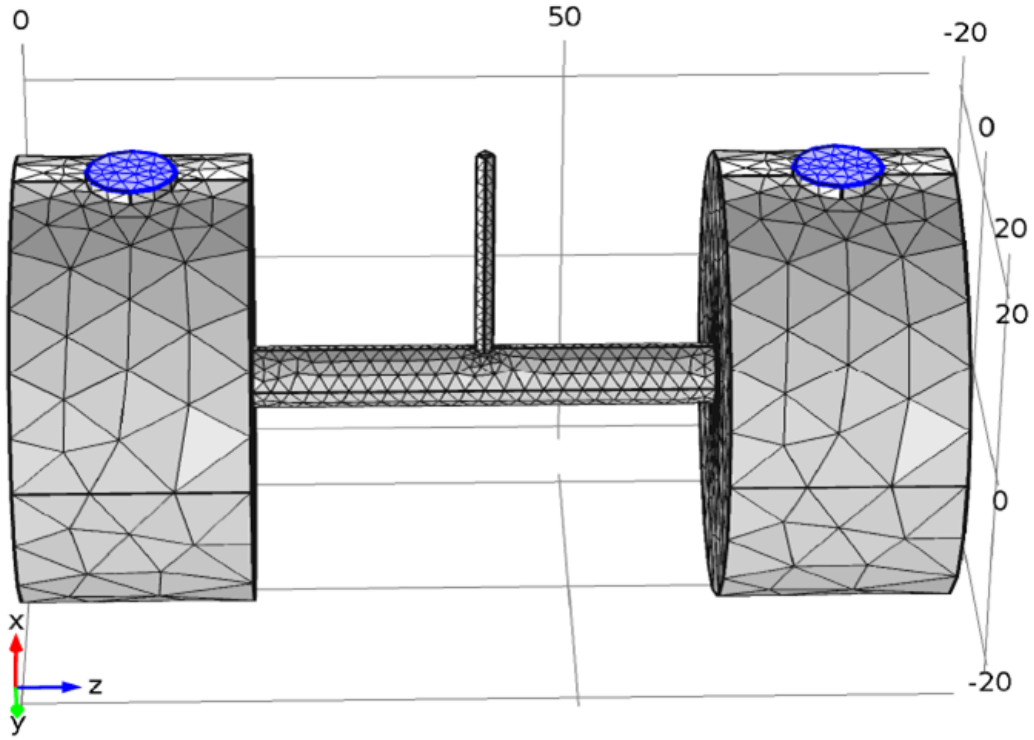


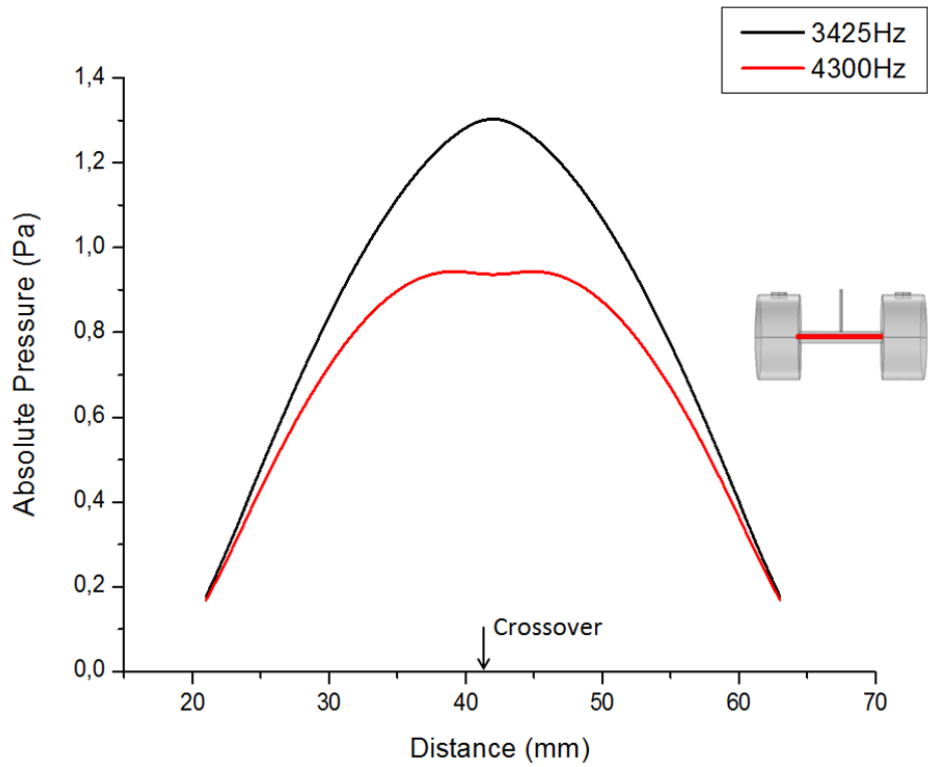
Figure 21: Meshed geometry of the cell T-42-21-1.5. The mesh is built up by triangular and tetrahedral elements.

The solution time for this geometry with 10325 elements on a Intel[®] Core[™] i7 at 2,8 GHz and a main memory of 4 GB is 16 seconds. The problem was solved for the first six Eigenfrequencies wherein the first two are of interest. For this frequencies also the size of the finite elements are optimized as said before.

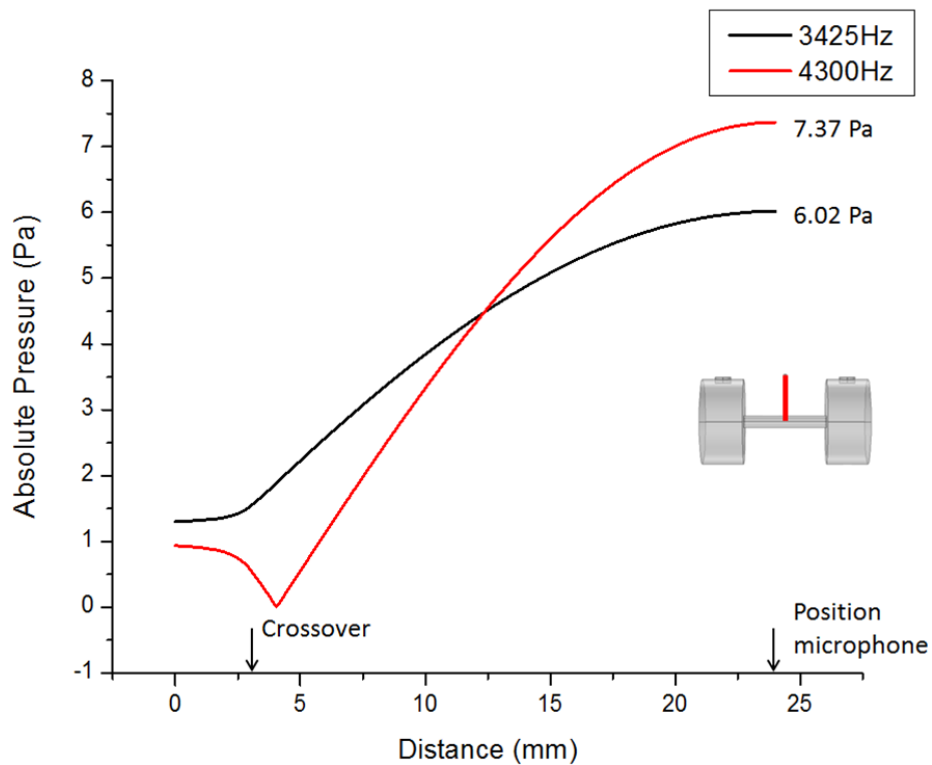
3.3.4 Results

In COMSOL are many different possibilities to visualize the results of the calculation as said before. For an adequate rating of the different cell designs the resulting acoustic pressure at the position of the microphone and the resonance frequencies are analyzed. The resonant tube system was designed for a working frequency of about 4000 Hz. The numerical calculation has as results one resonance beneath (3425 Hz) and one above (4300 Hz) the working frequency. Both are resonances of the whole tube system. Because of the different pressure distributions of them in the absorber and the resonator their origin can be identified. The first Eigenfrequency has a higher pressure amplitude in the middle of the absorber and a lower one in the resonator than the second one. Figure 22 (a) shows the absolute pressure along the axis of the absorber. The shape of the curve shows that the resonance at 3425 Hz is similar to the pressure field of a both ends open cylindrical resonator. In figure 22 (b) the resonance at 4300 Hz could be compared to the pressure field of a one side open cylindrical resonator. This can be identified by the minimum of the pressure near the crossover from the absorber to the resonator. The most important knowledges are:

- The resonance at 3425 Hz has its origin in the absorber and the acoustic pressure is transported in the resonator to the position of the microphone.
- The resonance at 4200 Hz has its origin in the resonator and is amplified by the acoustic pressure field of the absorber.
- Both occur because of a combination of the two cylindrical resonators.



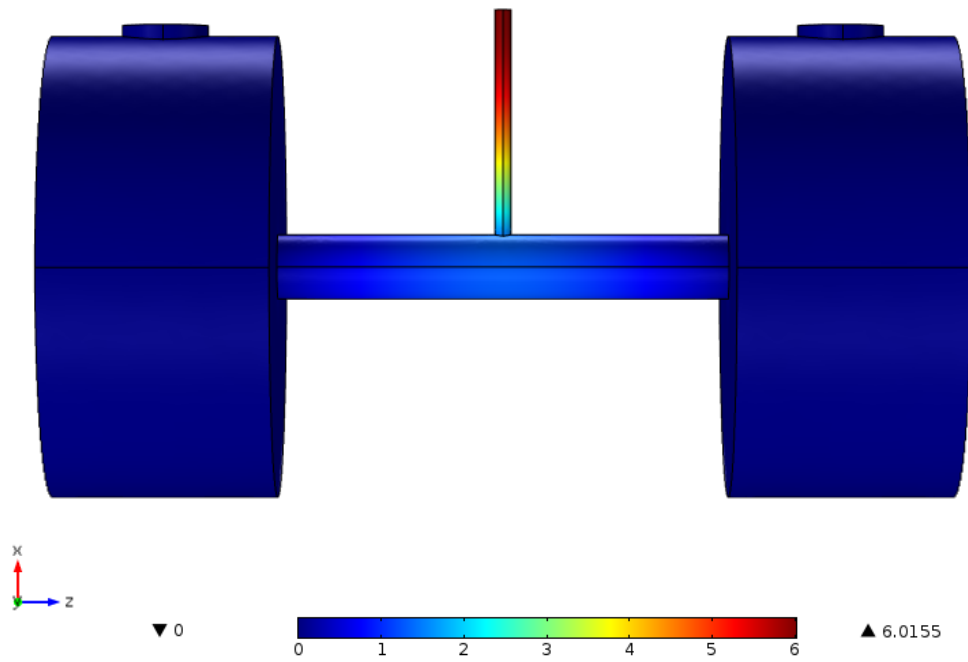
(a)



(b)

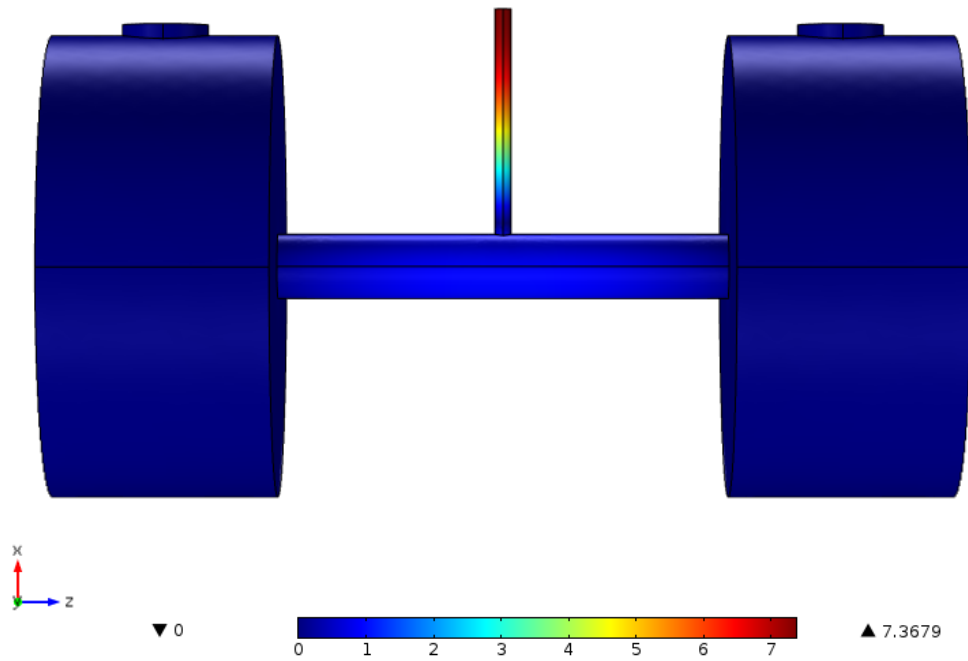
Figure 22: Absolute pressure of the first and second Eigenfrequency of the cell T-42-21-1.5 along the respective cylinder axis. (a) shows the pressure along the axis of the absorber and (b) along the axis of the resonator. The first 3 mm in (b) are a part of the absorber.

Surface: Absolute pressure @ 3425 Hz (Pa)



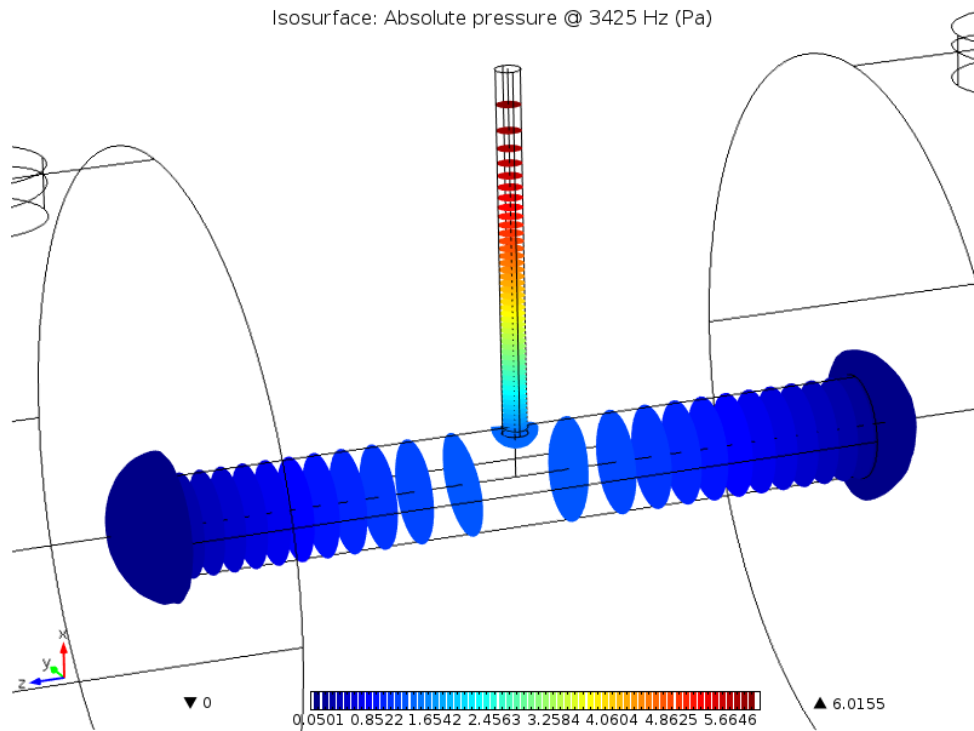
(a)

Surface: Absolute pressure @ 4300 Hz (Pa)

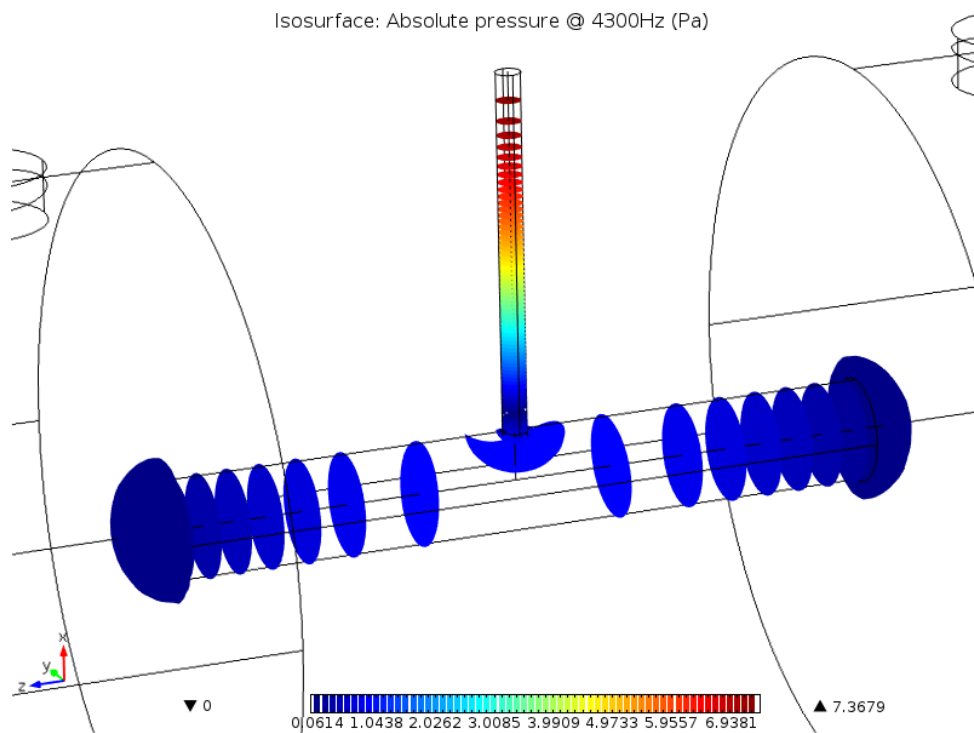


(b)

Figure 23: Absolute pressure of the first (a) and second (b) Eigenfrequency of the cell T-42-21-1.5 on the surface.



(a)



(b)

Figure 24: Absolute pressure of the first (a) and second (b) Eigenfrequency of the cell T-42-21-1.5. Displayed are the iso-surfaces of equal pressure in the cell. A difference of the pressure field at the crossover can be seen and compared with figure 22.

3.3.5 Simulated geometries

The following tables gives an overview of the simulated cell geometries. In table 2 are all T-resonators listed. The calculated models of the T-resonator geometries are set up as in the example before. The influence of the change of the dimensions absorber length, resonator length and diameter of resonator are studied.

Table 2: Cell dimensions of simulated T-resonators

L_a ... Length of absorber

L_r ... Length of resonator

D_r ... Diameter of resonator

Name	L_a [mm]	L_r [mm]	D_r [mm]	Name	L_a [mm]	L_r [mm]	D_r [mm]
T-21-21-0.5	21	21	0.5	T-21-42-0.5	21	42	0.5
T-21-21-1	21	21	1	T-21-42-1	21	42	1
T-21-21-1.5	21	21	1.5	T-21-42-1.5	21	42	1.5
T-21-21-2	21	21	2	T-21-42-2	21	42	2
T-21-21-2.5	21	21	2.5	T-21-42-2.5	21	42	2.5
T-21-21-3	21	21	3	T-21-42-3	21	42	3
T-21-21-3.5	21	21	3.5	T-21-42-3.5	21	42	3.5
T-21-21-4	21	21	4	T-21-42-4	21	42	4
T-42-21-0.5	42	21	0.5	T-42-42-0.5	42	42	0.5
T-42-21-1	42	21	1	T-42-42-1	42	42	1
T-42-21-1.5	42	21	1.5	T-42-42-1.5	42	42	1.5
T-42-21-2	42	21	2	T-42-42-2	42	42	2
T-42-21-2.5	42	21	2.5	T-42-42-2.5	42	42	2.5
T-42-21-3	42	21	3	T-42-42-3	42	42	3
T-42-21-3.5	42	21	3.5	T-42-42-3.5	42	42	3.5
T-42-21-4	42	21	4	T-42-42-4	42	42	4

Name	L_a [mm]	L_r [mm]	D_r [mm]	Name	L_a [mm]	L_r [mm]	D_r [mm]
T-63-21-0.5	63	21	0.5	T-63-42-0.5	63	42	0.5
T-63-21-1	63	21	1	T-63-42-1	63	42	1
T-63-21-1.5	63	21	1.5	T-63-42-1.5	63	42	1.5
T-63-21-2	63	21	2	T-63-42-2	63	42	2
T-63-21-2.5	63	21	2.5	T-63-42-2.5	63	42	2.5
T-63-21-3	63	21	3	T-63-42-3	63	42	3
T-63-21-3.5	63	21	3.5	T-63-42-3.5	63	42	3.5
T-63-21-4	63	21	4	T-63-42-4	63	42	4
T-84-21-0.5	84	21	0.5	T-84-42-0.5	84	42	0.5
T-84-21-1	84	21	1	T-84-42-1	84	42	1
T-84-21-1.5	84	21	1.5	T-84-42-1.5	84	42	1.5
T-84-21-2	84	21	2	T-84-42-2	84	42	2
T-84-21-2.5	84	21	2.5	T-84-42-2.5	84	42	2.5
T-84-21-3	84	21	3	T-84-42-3	84	42	3
T-84-21-3.5	84	21	3.5	T-84-42-3.5	84	42	3.5
T-84-21-4	84	21	4	T-84-42-4	84	42	4

For the comparison of the T-resonator and the cell dimensions of the Micro Soot Sensor (MSS) also simulations have been done. In table 3 are further cells listed where combinations of T-resonator systems are combined with $\frac{\lambda}{2}$ and $\frac{\lambda}{4}$ cylindrical volumes. A higher acoustic signal by a combination of several T-resonators could not be observed. More detailed results of the simulation are given later at the comparison of the results of the calculation and the experiments.

Table 3: Combination of T-resonator and cylindrical volumes

Name	Description
MSS	Both ends open cylinder as resonator.
PT-42-21-x	Two T-resonators aligned and connected with a Notch-filter. The diameter of the resonator x is varied (0.5 mm - 4mm step width 0.5)
PT-42-21-x asym	Same geometry as MSS but instead of the cylindrical resonator a T-resonator is used. Also with a variation of the diameter x as above.

4 Experimental evaluation of different cell designs

In this section the photoacoustic measurements on different cell designs will be described. For the evaluation of the pure photoacoustic signal and its quality no other effects should give influences on it. A well-known effect at the AVL's Micro Soot Sensor is the window pollution by soot particles during long time measurements. These soot particles could give a disturbing photoacoustic signal if they are located in the laser beam. So NO_2 was used as acoustic transducer in stainless steel prototypes and also in prototypes made in a 3D-Printer at the Institute of process engineering of the TU Graz.

4.1 Conventional - Prototyping and Rapid - Prototyping

Prototyping is a very important section during a development process. As in that case no device could be built up only on the results of numerical calculations. These results have to be checked with the results of measurements. Therefore prototypes were constructed and manufactured.

The requirements on the prototypes refers to the acoustic behaviors. Usually prototypes for applications like the photoacoustic are made out of stainless steel or similar materials which could be tooled by specific machines. Therefore special technical drawings have to be prepared regarding to the possibility to manufacture it. This will always take time, good knowledge of production engineering and a lot of experience of the technical drawer as well. The advantages of this method are high precision, high polished surfaces, low manufacturing tolerances and good mechanical properties related to the material. Disadvantages are high costs, the know how for the drawings and the manufacturing and it takes often a lot of time.

The requirements for a resonant photoacoustic cell are thick walls that no structure-borne noise could occur. Further smooth surfaces are necessary that the acoustic surface losses are small as possible and particle deposition could be minimized. The last point is an important requirement for a cell for determining the soot mass concentration in exhausts. In the comparing measurements of different cells the sample gas is NO_2 . Particle deposition does not occur in that case. Referring the sample gas the cell material has to be inert otherwise oxidation or reduction processes may manipulate the analyt. The cell made out of stainless steel can be seen in figure 25.

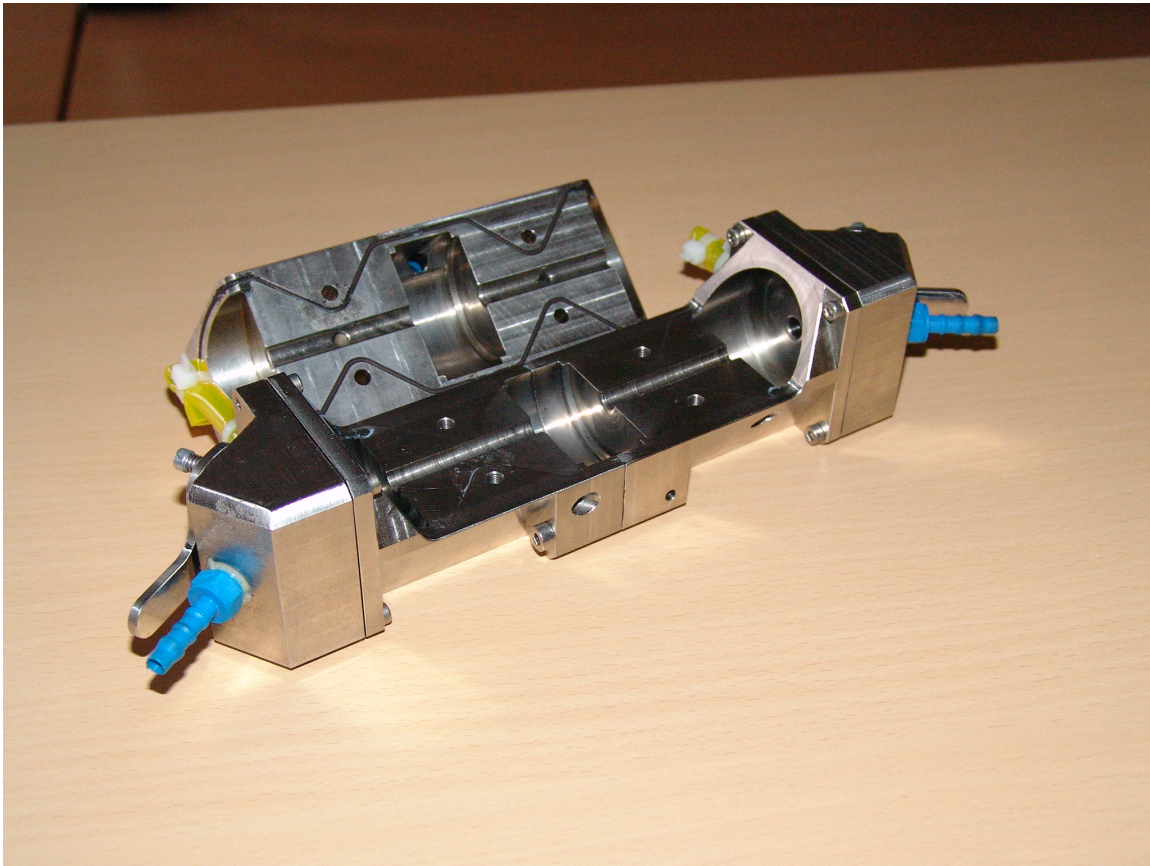


Figure 25: Stainless steel cell PT-42-21-x with the removed upper shell.

As described above the requirements on the cell give the possibility to use another kind of prototyping. At the institute of precision engineering a 3D printer (zPrinteer450) could be used for rapid prototyping. The technical key data for the printer are [23]

- resolution: 300 x 450 dpi
- partially model-size: 203 x 254 x 203 mm
- layer thickness: 0.089 - 0.102 mm
- formats: stl / vrml / 3ds / ply

The printer uses a technique where a binder is printed on a thin layer of plastic powder. Each layer represents a cross-section of the model. After the printing procedure the rest of the plastic powder could be blown of. In a post process the model surface has to be treated with cyanoacrylate for better mechanical properties. The prototype could be seen in figure 26. The outer surface of this cell differs to them of the stainless steel one, but

the inner volume is equal. The surface is rough but could be polished that it is smooth enough. The first experiments with this cell has been done one month after production. Another rapid prototyped cell were used directly after production. An reduction at the inner cell surface could be observed at the cells that where used directly after processing. The cyanoacrylate is hydrophilic and needs water to become end stiffness. The NO_2 sample gas reacts with the H_2O molecules at the inner surface of the cell 30.



The produced nitric acid was not verified analytical but the inner surface of the cell was colored yellow instead of white after the measurement and the cell had an acid smell. The reduction of the NO_2 reduces the concentration of it in the sample gas and the photoacoustic signal was smaller then expected. This chemical reaction doesn't occur in the cell which was used after a storage time. During the storage time the water could be evaporate or react with the cyanoacrylate.



Figure 26: Rapid prototyped cell PT-42-21-x

In figure 27 the photoacoustic signals in different prototyped cells are shown. All the resonators have the same dimensions with an absorbing section of 42 mm length and a diameter of 6 mm. The crossover to the resonator has an trumpet like shape. The length of the resonator is 21 mm and has a diameter of 1.5 mm. The NO_2 concentration was equal and the laser beam was irradiated in the same way. For the detection was the same microphone used.

Differences of the signal heights have several reasons. The stainless steel prototype delivers an acoustic signal with a height of 0.43 V. This signal intensity was observed several times. Both plastic cells have problems to reach the same intensity as the stainless steel one. As described before the surface of them is more rough and acoustic losses can damp the signal. Moreover this cells do not have the same tightness. Because of the sample gas, which is stored in a pressure vessel, it is only possible to pump it into the cells. For the use in soot measurements the cells are designed to suck through them. All prototypes have the same tightness at under pressure but different at over pressure. The plastic cell are not tight enough and will loose sample gas during sampling. The noisy signal of the humid plastic cell has its origin at the chemical reaction as described before.

The peak position of the resonances is at the stainless steel and the dry plastic cell the same. The peak position of the humid cell is not really clear because of the noisy signal trend. Under the acceptance of the reduction of the NO_2 the composition of the sample gas is changed. This will have an effect on the speed of sound in the medium and so the the longitudinal oscillations will appear at different frequencies.

For determining the Eigenfrequency spectrum of a cell it is possible to use prototypes made out of plastic. The big advantage are the costs but the resulting pressure differs to much to them of the stainless steel cell. Further the plastic material has to be aged or preheated before using it together with NO_2 . Exhausts are complex aerosols with different gas compositions and a lot of aggressive acids inside. To measure such aerosols plastic cell from such a 3D printer are not really useable.

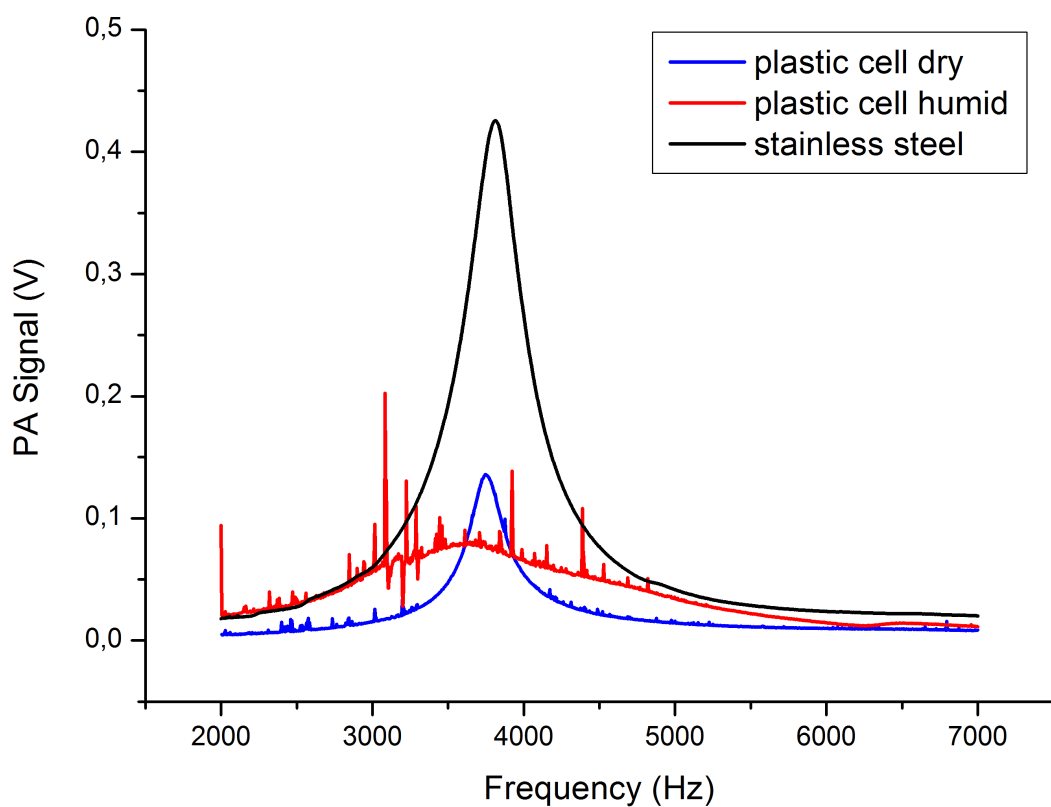


Figure 27: Photoacoustic signal in a stainless steel and a plastic (humid and dry) cell

4.2 Setup

A measuring device for exhausts will always have the problem of pollution by deposited particles in the system. This could happen by thermophoresis, impaction and adhesion of particles. For the quantification of the different cell shapes any pollution effect should be avoided so a particle free sample gas is used. The Eigenfrequency spectrum of a cell is only shifted a little bit by the use of different sample gases because of different speed of sounds. The relative peak position of the Eigenfrequencies are not influenced.

For the experiments a 1000ppm NO_2 sample mixed gas has been used. NO_2 has an absorbing maximum at a wavelength of about 450 nm [16]. For the detection of the soot mass concentration in an aerosol a diode laser with a wavelength of 808 nm hits only a small local maximum of NO_2 [22]. For the experimental setup a 405nm diode-laser from Qioptics is used which hits the very broad maximum which can be seen in figure 4.

The different cells are mounted at a so called "bread board" which is a part of the optical bench. The optical bench was necessary to collimate the laser beam by a lens system. It should also guarantee that the beam cross-section is at all cells equal and an influence of it could be neglected. The collimated beam has not at all parallel rays. The rays are converging a little that they could not hit the walls. This is necessary to be always on the safe side.

The beam enters and exits the cell over a window which is mounted oblique to the horizontal axis of the cell. This should give the possibility to purge the windows with filtered air. This feature is not necessary for the detection of NO_2 but for aerosols. The geometry has an influence on the resonance behavior so the feature is already implemented in the cell construction. The sheath air has a continuous flow and dilutes the exhaust after the measuring section.

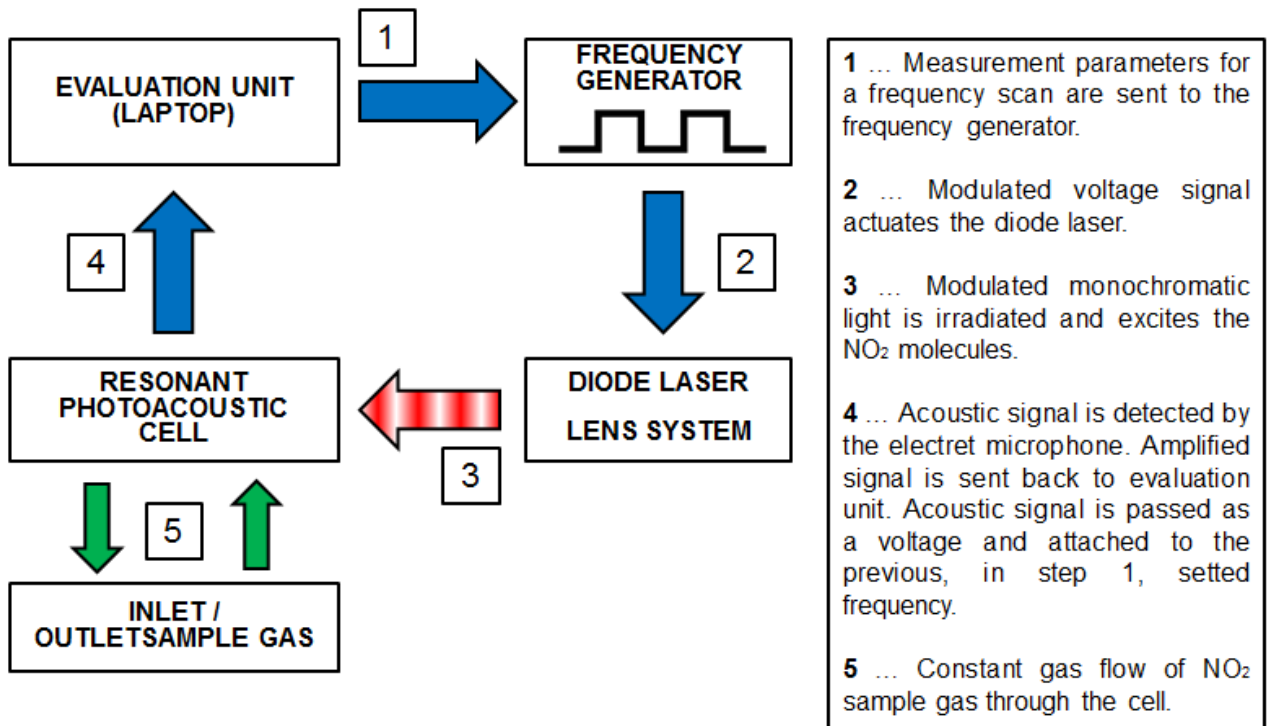


Figure 28: Principle sketch of the experimental setup for the determination of the frequency spectra of different photoacoustic cells.

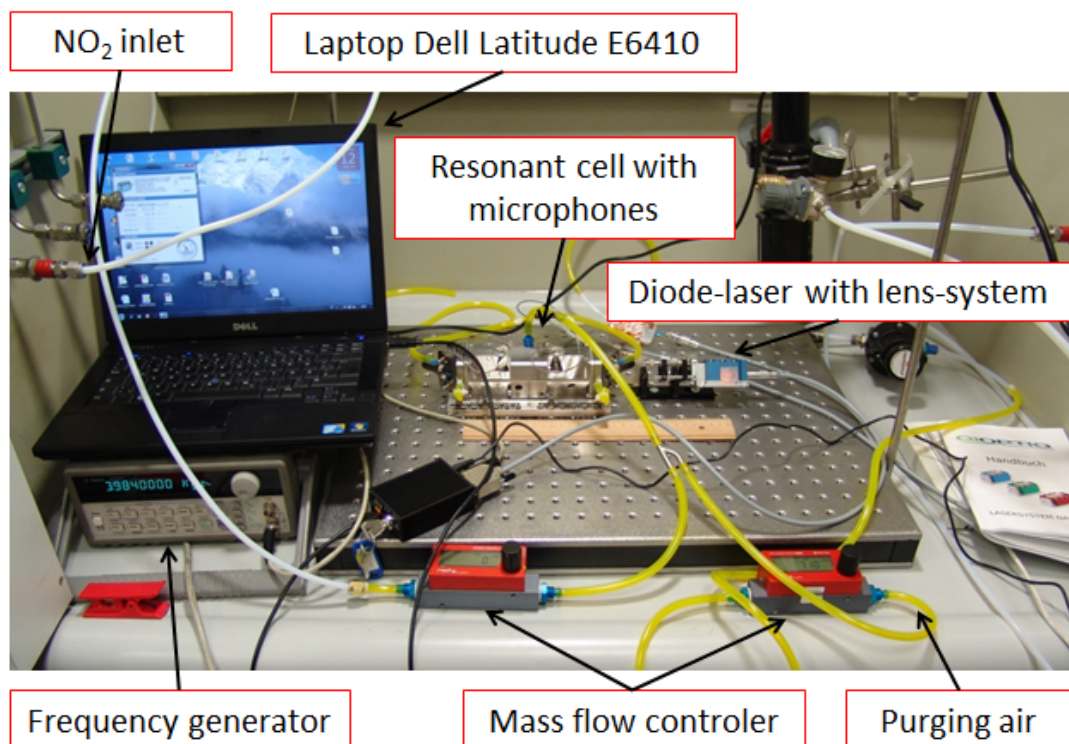


Figure 29: Experimental setup for the determination of the frequency spectra of different photoacoustic cells.

4.2.1 Data logging

For the detection of the produced acoustic signal an electret microphone from Knowles is used. This type of microphone is also in the Micro Soot Sensor in use and so the detected signals of the different cells could be compared. The microphone is mounted on a board where the signal is enhanced by a value of ten. The signal will be sent to an analog - digital converter from National Instruments. The converted signal is read with a frequency 125 kHz by the "Data Acquisition Assistant" of the measure and control software (LabView) installed on a Dell E6410 laptop. Afterwards the signal is filtered by a second order Bessel band-pass filter where the upper and lower limits are plus minus 500 Hz of the actual frequency of the scan. Two microphones could be analyzed at the same time with the same priority. The channels which are analyzed are the system time, the frequency of the laser which is set by the program, the by the microphone detected frequency, the FFT sound level, the peak to peak value of the signal, the peak value and the rms-value. All these values are handed over to the logging module in the program. The data set is stored as .txt files.

For a frequency scan the program controls the diode-laser over a frequency generator. The frequency range, the step width and the stabilization time for each point are set in the program. The frequency generator is triggered over a RS232 connection. The diode-laser needs an upper and lower voltage limit for modulating a signal which is set manually at the frequency generator. The signal shape could also be selected in the program (e.g. rectangle, triangle and a ramp).

4.3 Measurements

Regarding to the results of the simulations the resonators T-42-21-3 and T-42-21-1.5 seems to bring the best results in comparison to the resonant cell of the Micro Soot Sensor. Different cell geometries where tested with the described measurement setup. The following table 4 gives an overview of the tested cells. The full results of the evaluation of different T-resonators is shown later.

Table 4: Tested cell geometries

Name	Characteristics
PT-42-21-x (steel)	Two T-resonators aligned and connected with a Notch-Filter. The diameter of the resonator x is varied (1.5, 2, 2.2, 3 mm).
PT-42-21-x (rapid prototype)	Two T-resonators aligned and connected with a Notch-Filter. The diameter of the resonator x is varied (1.5, 2, 2.2, 3 mm).
Micro Soot Sensor	Cylindrical resonator



Figure 30: Polyetheretherketon PEEK insert to make the resonator diameter smaller from 3 mm to 1.5 mm

At the first measurements three significant peaks could be detected in a frequency range of 2000 Hz to 7000 Hz with the PT-42-21-3. The resolution of such a scan has a step width of 1Hz. The first two oscillations in the spectrum are longitudinal one in the T-shaped resonator system at 3172Hz and 4552Hz with a height of 0.206 Volts and 0.247 Volts. This is the voltage that is produced by the acoustic pressure on the electret microphone at a specific frequency. The third and smallest one is a radial oscillation in the porous inlet ring which can be seen in figure 31 as a shoulder at the trailing edge of the second peak at 4896Hz with a height of 0.151 Volts. This peak can be used as a marker because it is not influenced by the change of the diameter of the resonator. The first comparison with the cell of the Micro Soot Sensor shows that the detected acoustic signal of the first peak of PT-42-21-3 is lower than the single resonance of the MSS at 4044Hz and with a height of 0.245 Volts. The second peak of the prototype is as high as this single resonance of the MSS. Depending on the NO₂ concentration one time the second resonance of the prototype cell delivers a little bit higher signal and one time the MSS cell. The flow was by the use of floating body flow meter not stable enough to eliminate this small fluctuations. These PT-42-21-3 is already not an improvement related to the resonator generated acoustic pressure field. But the T-shape gives the possibility to place the microphone not directly to the exhaust path.

The next step is to use the insert cylinders within the stainless steel cell. The frequency spectrum consists of one peak at 3812Hz with a height of 0.426 Volts and one at 4896Hz with a height of 0.046 again in the trailing edge. The peak height of the photoacoustic signal is 2 times higher than the prior tested PT-42-21-3 and the MSS which can be seen in figure 31. Also the radial oscillation at the inlet cylinder is smaller then before but at the same frequency.

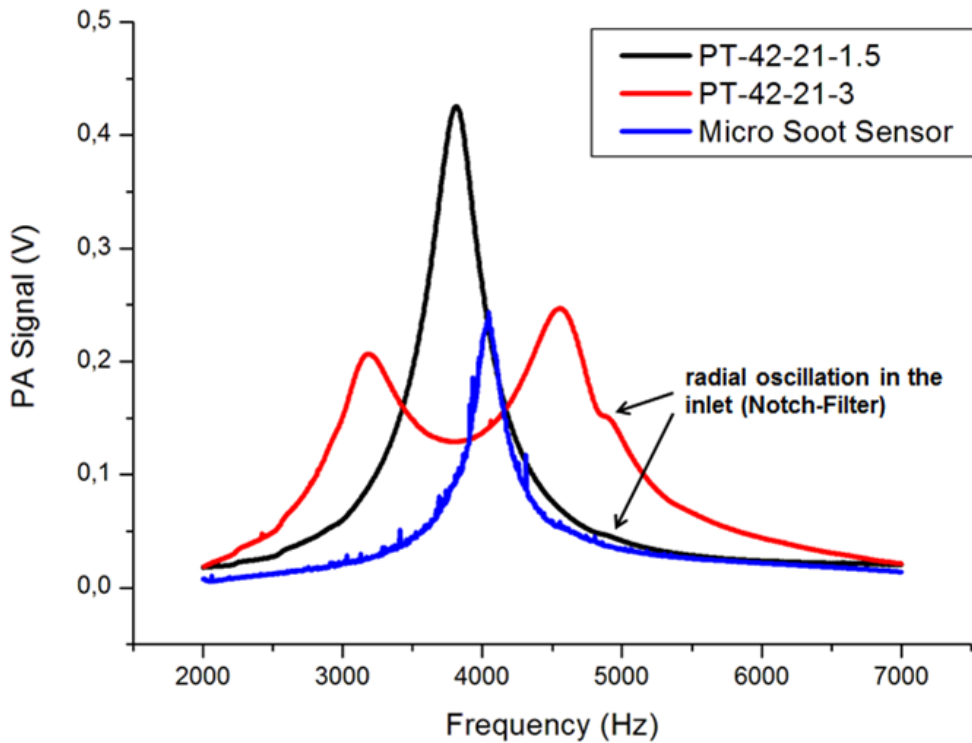


Figure 31: Photoacoustic signal enhanced by PT-42-21-x with different resonator diameters x and the Micro Soot Sensor

When the resonator diameter becomes smaller another frequency spectra is detected than expected. The results of the simulations show that there should be also two resonances were the first should appear at a lower frequency and the second at a higher one. Both with a little higher acoustic pressure field as produced with the resonator in the Micro Soot Sensor. To see what happen in detail when the resonator diameter is becoming smaller, two further cylindrical inserts made out of PEEK are manufactured with a diameter of 2 mm and 2.2 mm.

The frequency spectra of PT-42-21-2 and PT42-21-2.2 can be seen in figure 32 together with the spectra of PT-42-21-3 and PT-42-21-1.5. It can be seen that a becoming smaller diameter will shift the frequencies of the two longitudinal oscillations in the T-resonator system together. Due to acoustic losses, as described in the fundamentals, the peaks are broadened and an overlap of them could also be seen a diameter of 3 mm. At a diameter of 1.5 mm the two resonances could not be separated. For the construction no smaller diameter could be realized because the microphone itself has a small metal cylinder in front of the acoustic sensitive parts which has an outer diameter of 1.5 mm.

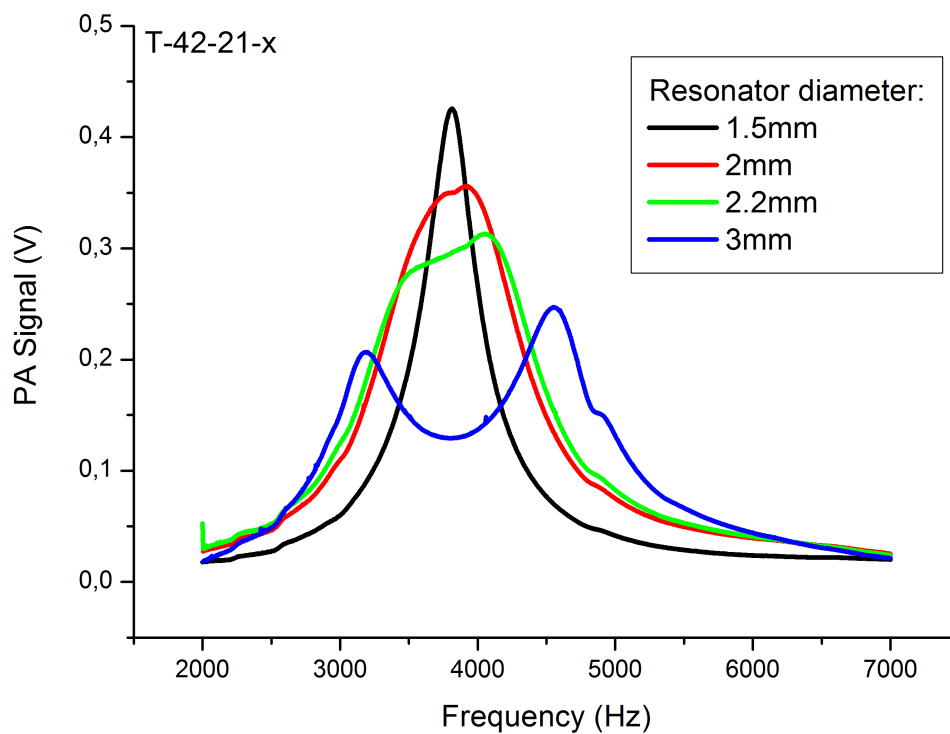


Figure 32: Overlap of the first and second Eigenfrequency by a becoming smaller diameter in T-resonator with a absorber length of 42 mm and a resonator length of 21 mm.

4.3.1 Variable T-Cell

As seen that a small variation of one degree of freedom has such an effect on the resulting acoustic pressure field a modifiable T-cell is constructed. With this cell it is possible to change the absorber length, the length of the resonator and its diameter. The realized sizes could be seen in table 5. Also the influence of the diameter of the absorber is analyzed but has no effect to the frequency spectrum of the cell but on the resulting pressure field. This results were compared with the results of the simulation which is figured out a section later.

Table 5: Cell dimensions of variable T-resonators L_a ... Length of absorber L_r ... Length of resonator D_r ... Diameter of resonator

Name	L_a [mm]	L_r [mm]	D_r [mm]	Name	L_a [mm]	L_r [mm]	D_r [mm]
T-21-21-1.5	21	21	1.5	T-21-42-1.5	21	42	1.5
T-21-21-2	21	21	2	T-21-42-2	21	42	2
T-21-21-3	21	21	3	T-21-42-3	21	42	3
T-21-21-4	21	21	4	T-21-42-4	21	42	4
T-42-21-1.5	42	21	1.5	T-42-42-1.5	42	42	1.5
T-42-21-2	42	21	2	T-42-42-2	42	42	2
T-42-21-3	42	21	3	T-42-42-3	42	42	3
T-42-21-4	42	21	4	T-42-42-4	42	42	4
T-63-21-1.5	63	21	1.5	T-63-42-1.5	63	42	1.5
T-63-21-2	63	21	2	T-63-42-2	63	42	2
T-63-21-3	63	21	3	T-63-42-3	63	42	3
T-63-21-4	63	21	4	T-63-42-4	63	42	4
T-84-21-1.5	84	21	1.5	T-84-42-1.5	84	42	1.5
T-84-21-2	84	21	2	T-84-42-2	84	42	2
T-84-21-3	84	21	3	T-84-42-3	84	42	3
T-84-21-4	84	21	4	T-84-42-4	84	42	4

The measurements with a absorption section diameter of 4 mm was only done with the cell T-42-21-x. The change of this value has no influence on the frequency spectrum. The higher detected pressure is a result of the minimized resonance volume at constant excitation, because the beam profile was not changed.

With this cells a clear context of the phenomenon should be found. The lengths listed in table 5 are related to the 4000 Hz. Regarding to the equation 21 the lengths are related

to multiples of a quarter wavelength of a acoustic standing wave in a cylindrical volume of 4000 Hz (e.g. 21 mm can be seen as $\lambda/4$, 42 mm as $\lambda/2$ and so on). By the change of the diameters the observed overlap of two resonances is investigated at different T-cell dimensions.

- In figure 33 and 34 are the results for a T resonator shown where the length of the absorption section is 21 mm and the length of the resonator is one time 21 mm and one time 42 mm. In both spectra several resonances are shown. The first two peaks are the longitudinal oscillation which are analyzed. The first oscillation is attenuated by a becoming smaller diameter. At a resonator length of 21 mm this oscillation appears at approximately 3500 Hz and moves with a becoming smaller diameter of the resonator to higher frequencies. The same applies for the cell with a resonator length of 42 mm. No amplification could be observed.
- In figure 35 are the results for a T resonator shown where the length of the absorption section is 42 mm and the length of the resonator is 21 mm. Figure and 36 shows the results for the same cell with a smaller diameter of the absorption section with 4 mm. The overlap of the frequencies and the amplification of the acoustic pressure of the signal could also be shown. The further amplification due to a smaller diameter of the absorber is only a result of the smaller volume. The laser beam cross-section has the same size as at the other measurements. The acoustic signal is less diluted then at the others.
- In figure 37 and 38 are the results for a T resonator shown where the length of the absorption section is 63 mm and the length of the resonator is one time 21 mm and one time 42 mm. The behavior of this cells is almost the same as the cells T-21-21-x and T-21-42-x. The difference is that the second oscillation becomes smaller with a becoming smaller resonator diameter.

- In figure 39 and 40 are the results for a T resonator shown where the length of the absorption section is 84 mm and the length of the resonator is one time 21 mm and one time 42 mm. The cell with the dimensions T-84-21-x shows the same behavior as the cell T-21-21-x and the others. One of the two oscillations disappear by becoming smaller resonator diameter. At the dimensions T-84-42-x a similar an overlap of the two longitudinal oscillations could be observed. Also the signal was amplified. By the fact that the dimensions of the cell are a multiple of the T-42-21-x this behavior was not surprising. The phenomenon occurs at above 2000 Hz. By doubling the lengths the resonance peaks appear at the half frequency. This results are confirmed by numerical calculations and are shown in the next section.

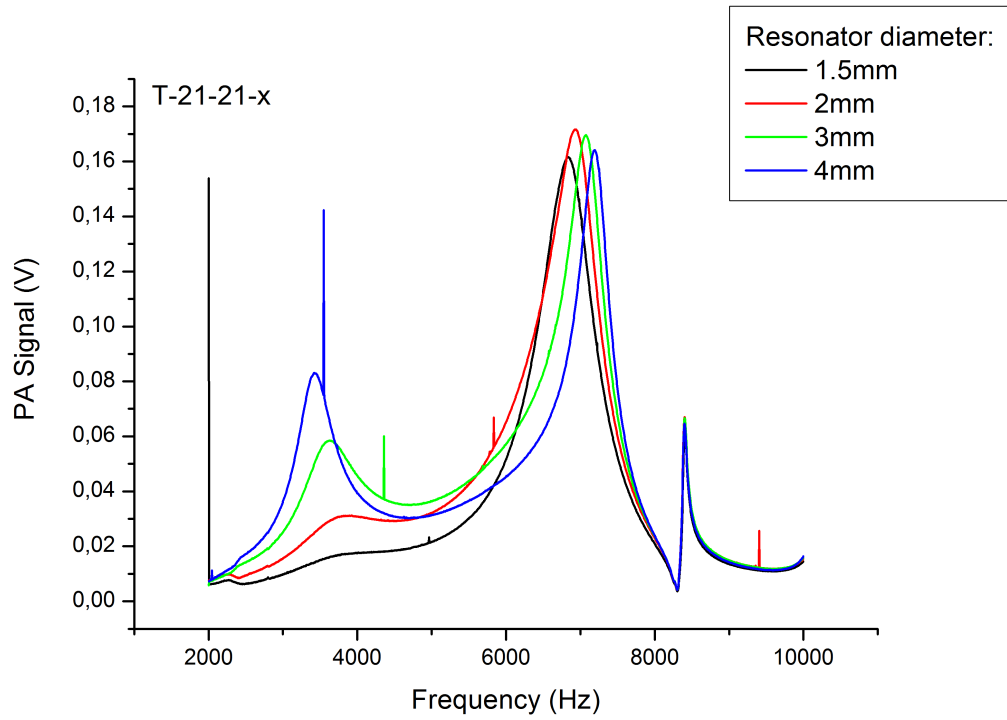


Figure 33: Resonance spectra of T-resonator with a absorber length of 21 mm and a resonator length of 21 mm with different resonator diameters.

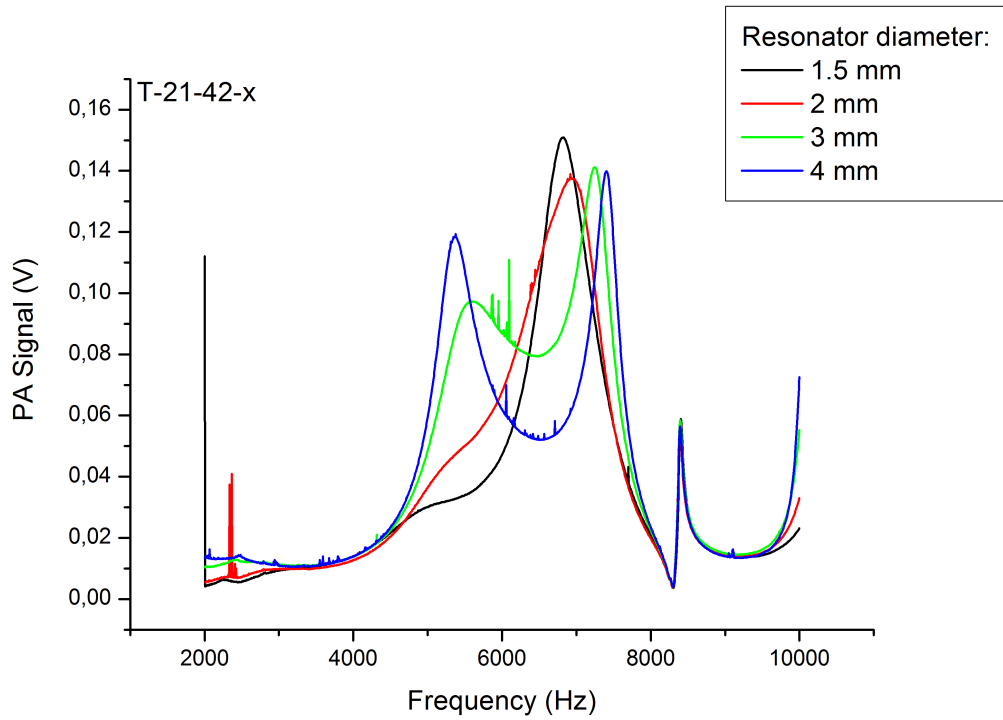


Figure 34: Resonance spectra of T-resonator with a absorber length of 21 mm and a resonator length of 42 mm with different resonator diameters.

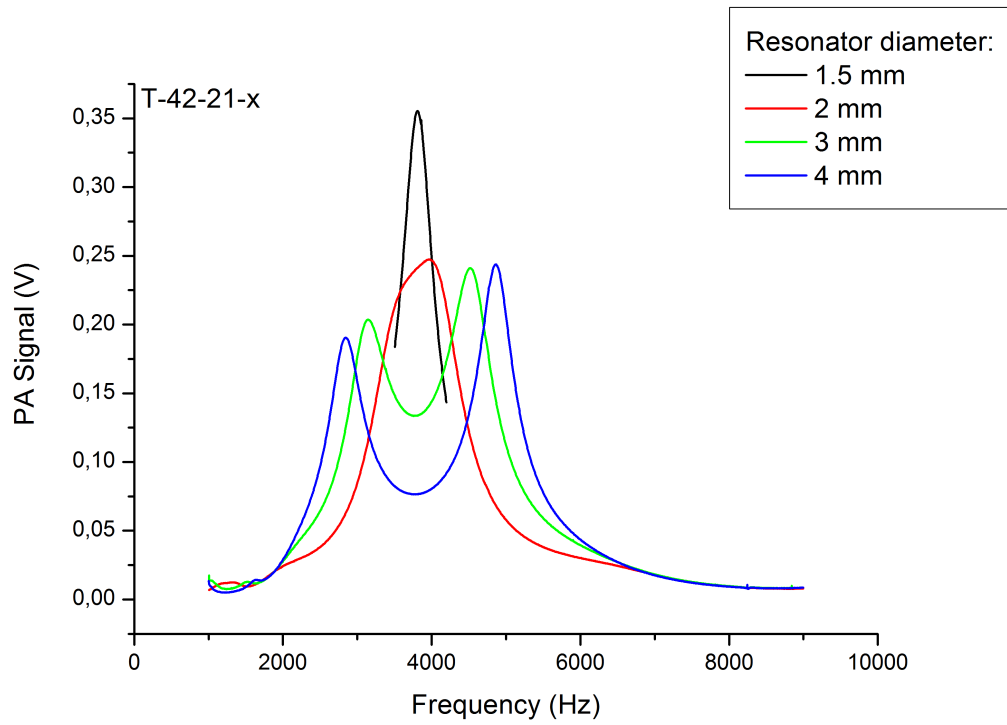


Figure 35: Resonance spectra of T-resonator with a absorber length of 42 mm and a resonator length of 21 mm with different resonator diameters.

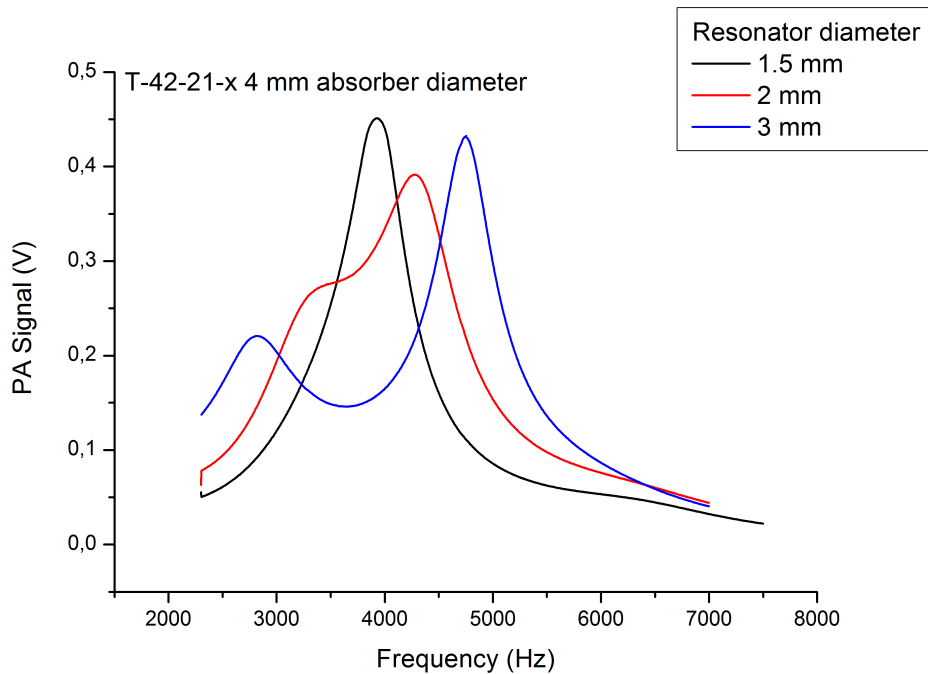


Figure 36: Resonance spectra of T-resonator with a absorber length of 42 mm, a resonator length of 21 mm, an absorber diameter of 4 mm and with different resonator diameters.

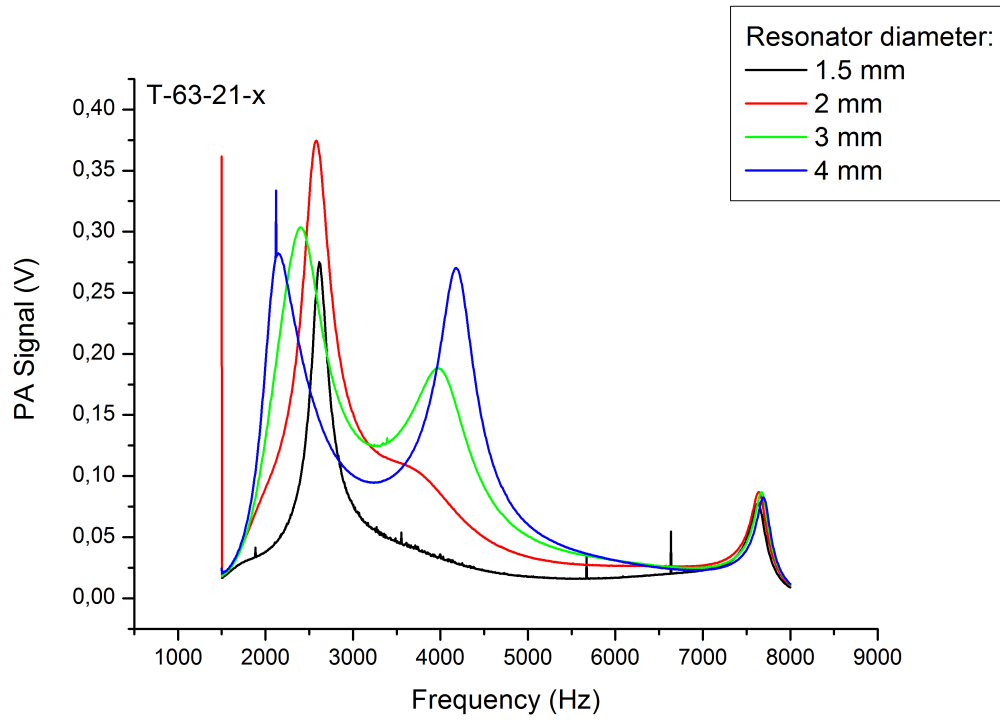


Figure 37: Resonance spectra of T-resonator with a absorber length of 63 mm and a resonator length of 21 mm with different resonator diameters.

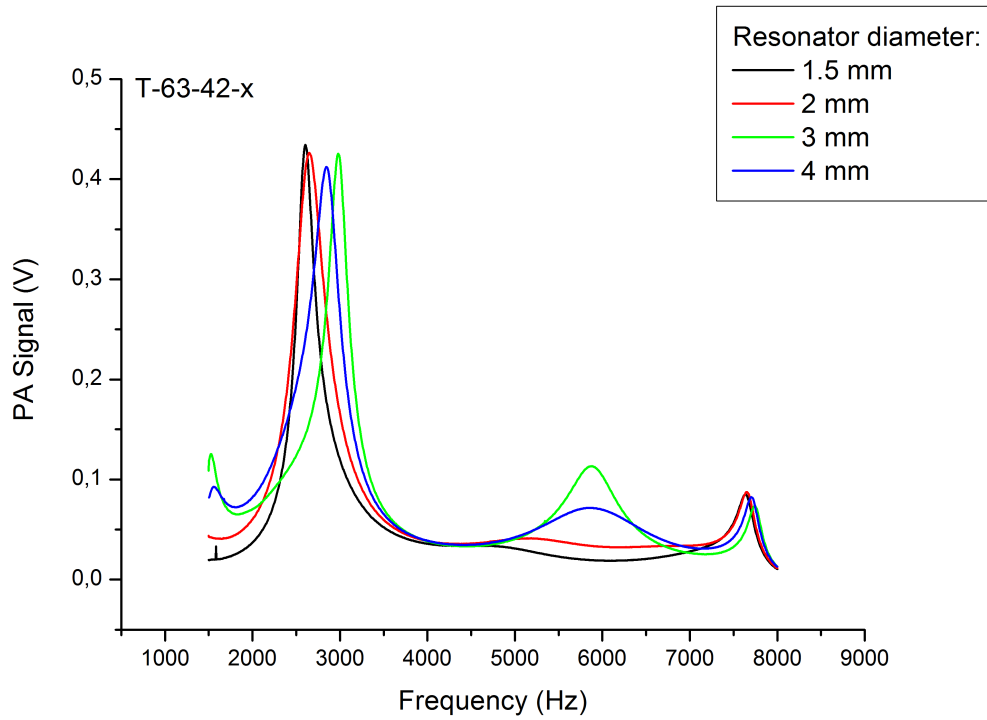


Figure 38: Resonance spectra of T-resonator with a absorber length of 63 mm and a resonator length of 42 mm with different resonator diameters.

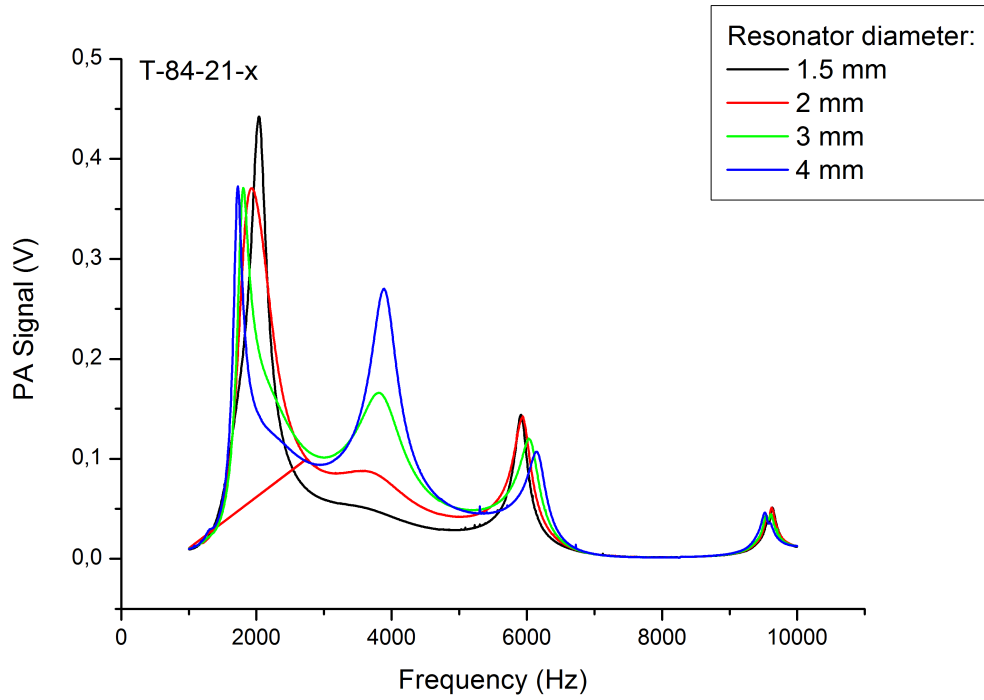


Figure 39: Resonance spectra of T-resonator with a absorber length of 84 mm and a resonator length of 21 mm with different resonator diameters.

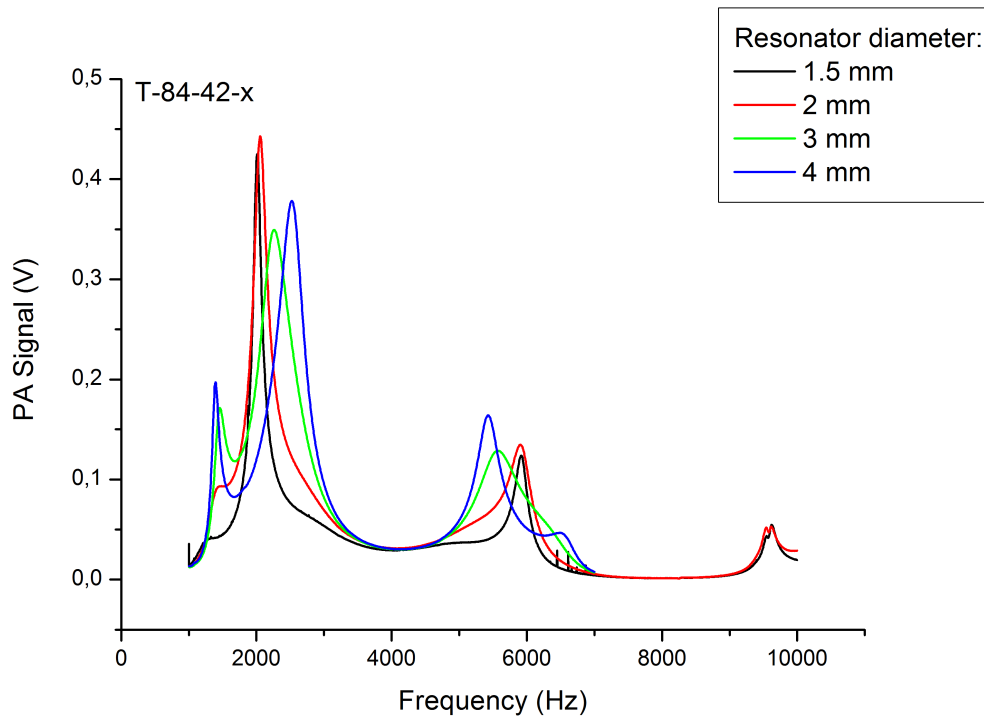


Figure 40: Resonance spectra of T-resonator with a absorber length of 84 mm and a resonator length of 42 mm with different resonator diameters.

4.3.2 Conclusion of measurements

The double T-resonator cell PT-42-21-3 has two significant peaks under and above the planned working frequency of 4000 Hz. By the usage of a smaller resonator diameter of 1.5 mm only one resonance peak was detected. The peak height is 1.2 to 1.5 times higher than the higher peak of PT-42-21-3. The origin of this phenomenon can be explained by a movement of the two Eigenfrequencies by a becoming smaller resonator diameter. The first Eigenfrequency is shifted to higher frequencies and the second Eigenfrequency is shifted to lower ones.

For a fully understanding of the resonance spectrum of T-resonator a variable T-cell was constructed. By a change of the length of the absorber and the resonator and its diameter the T-resonator was characterized. An overlap of the first and second Eigenfrequency can be detected if the length of the absorber and the length of the resonator have a ratio of about 2:1 and the diameter of the resonator is smaller than 2.2. By this overlap a amplification of the acoustic signal can also be detected.

5 Comparison of Simulation and Experiments

In this section the results of simulation and the experiments are compared. As described in a section before several influences on the acoustic standing wave are not considered in the simulations. So the simulation delivers a total mathematic solution where only sharp resonance peaks appear. In the experiment the photoacoustic effect, surface and volume losses of the acoustic signal, particle deposition in the measuring section, pressure changes and manufacturing precession will cause peak broadening. In the simulation the peak positions of the harmonics and their relative height were analyzed.

5.1 Different cell dimensions and the impact on the acoustic

In this section the influence of different ratios of geometric scales on the acoustic pressure field and the frequency spectrum are explained. For such a resonator no detailed research was done yet. Some experiments and simulations were done by Baumann [12]. This type of resonator was constructed under the respect of the idea of Helmholtz [20]. The developed T resonator could not be described at all with the formulas for common types of resonators like cylindrical volumes. But they are a good basement for the understanding of the T-shaped resonator.

At the beginning the influence of the diameter of the absorbing section is described. In this part of the measuring chamber the photoacoustic signal is generated. If the diameter of it becomes bigger the acoustic pressure that is only generated in the cross-section of the laser beam will be diluted by the bigger volume. Only if the beam cross-section becomes also bigger, there will be an improvement of the resulting acoustic pressure. The bigger volume of the absorption section has not an influence on the frequency spectrum of the cell. The observed frequency range was 2000 Hz and 7000 Hz. The Eigenfrequencies of the longitudinal standing waves are not influenced by a bigger or smaller diameter of the absorber. The upper limit of the diameter for determining the soot mass concentration is not set by acoustic behaviors. The bigger diameter needs higher velocities for equal gas exchange times. A higher speed of the aerosol may induce turbulences which are unwanted.

The length of the absorbing section is characterizing the position of the sum peak of the

first and second Eigenfrequency. By a becoming smaller resonator diameter the amplitudes of the first and second Eigenfrequency becomes higher. Further the first Eigenfrequency is shifted to higher frequencies and the second one is shifted to lower one. In the experiment both peaks overlap at a radius of 1.5 mm. With the equation 21 it is possible to find the resonance frequency of a T-shaped resonator with an infinitesimal small vertical resonator. From that point of view the length of the absorber has to fulfill the requirement that the device should work at 4000 Hz. In experiments with the variable T-cell, it could be shown that the concept of the T-cell works also at other frequencies for example 2000Hz. The resonator system for that frequency has an absorption section that has the doubled length of the realized one. The produced photoacoustic signal is much higher than in the cell with the dimensions optimized to 4000 Hz but it does not meet the requirements regarding the size and the working frequency.

In the vertical resonator no photoacoustic signal is generated. So it should be small as possible because the further volume in the whole resonant system will dilute the resulting pressure. This point of view applies when only one resonance is considered. The length of it is determined by the length of the absorbing section. If acoustical phenomena at the crossover regions, which can shift the Eigenfrequencies, are neglected absorber and resonator have to fulfill the ratio of 2:1. At this ratio both sections will behave like the former described cylindrical resonators - The absorber like a both ends opened pipe and the resonator as one with one end closed. Further the resonator has to be placed over the maximum of the longitudinal oscillation of the absorber. This could be shifted if the crossovers are not symmetrical. For example in one acoustic filter will be the inlet situated.

The influence of the diameter on the system could not be explained with the common theory. The experiments as well as the simulation results show that a becoming smaller diameter has an influence on the frequency spectrum. It shifts the lower longitudinal oscillation to higher frequencies and the upper one to lower frequencies but not in the same way.

Both resonances cause a higher acoustic pressure at the end of the resonator if the diameter becomes smaller. This effect was also verified with experiments and simulations. The following figures show the behavior of the former described parameter changes.

The figures 41 and 42 show the influence of a becoming smaller resonator to the frequency of the longitudinal oscillations in a T-shaped cell as shown in figure 18. The results of the experiments with NO_2 and the simulation are shown for two different cell dimensions. The figures 43 and 44 show the increasing pressure field at the position of the microphone. The results of the simulation could be compared with them of the experiments again. In the experiments the smallest use able diameter is 1.5 mm. Otherwise the small inlet cylinder, mounted on the microphone itself, doesn't fit into the resonator.

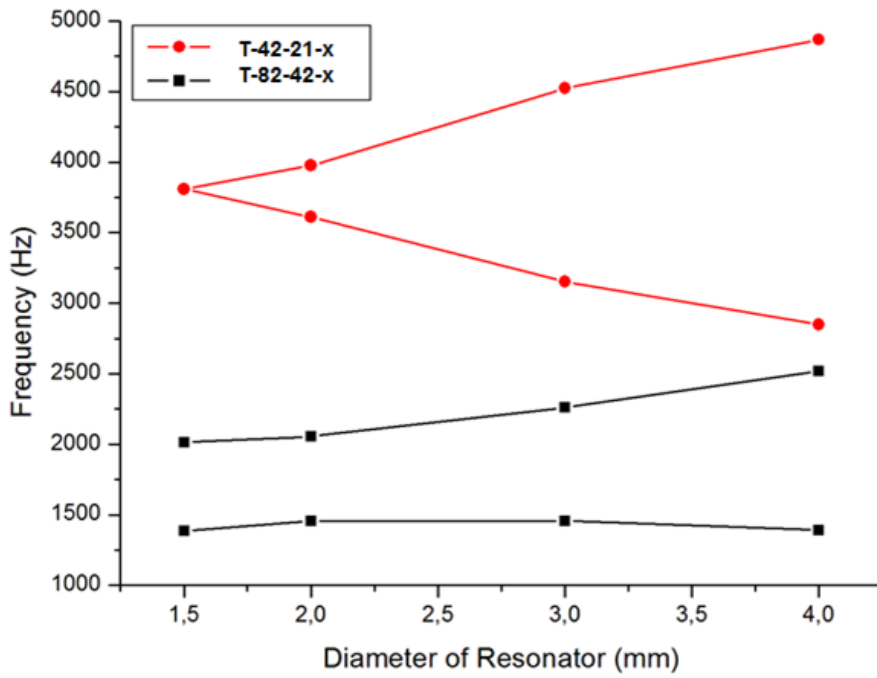


Figure 41: Results of experiments regarding the frequency shift of two T-resonators in addition of the resonator diameter. The absorber-resonator ratio is for both 2:1.

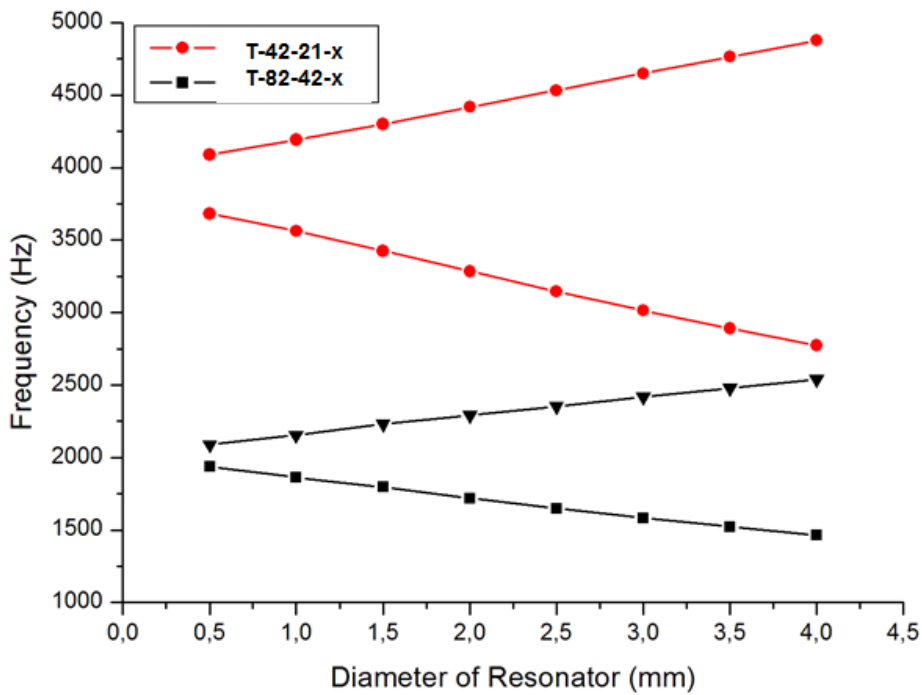


Figure 42: Results of simulation regarding the frequency shift of two T-resonators in addition of the resonator diameter. The absorber-resonator ratio is for both 2:1.

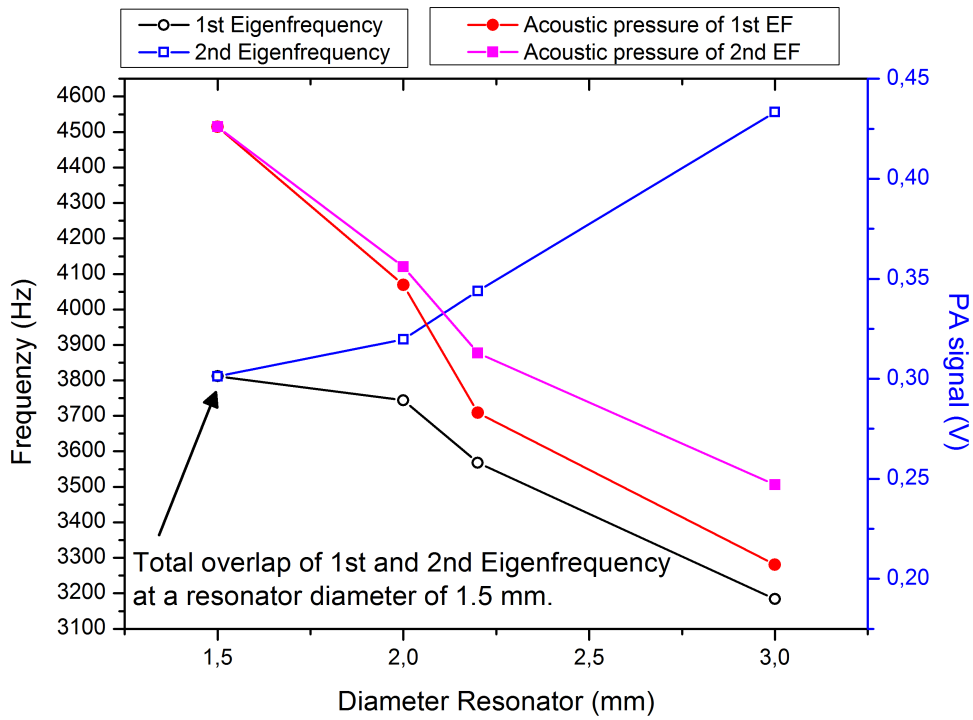


Figure 43: Frequency shift / pressure change in addition of the resonator diameter - experiment

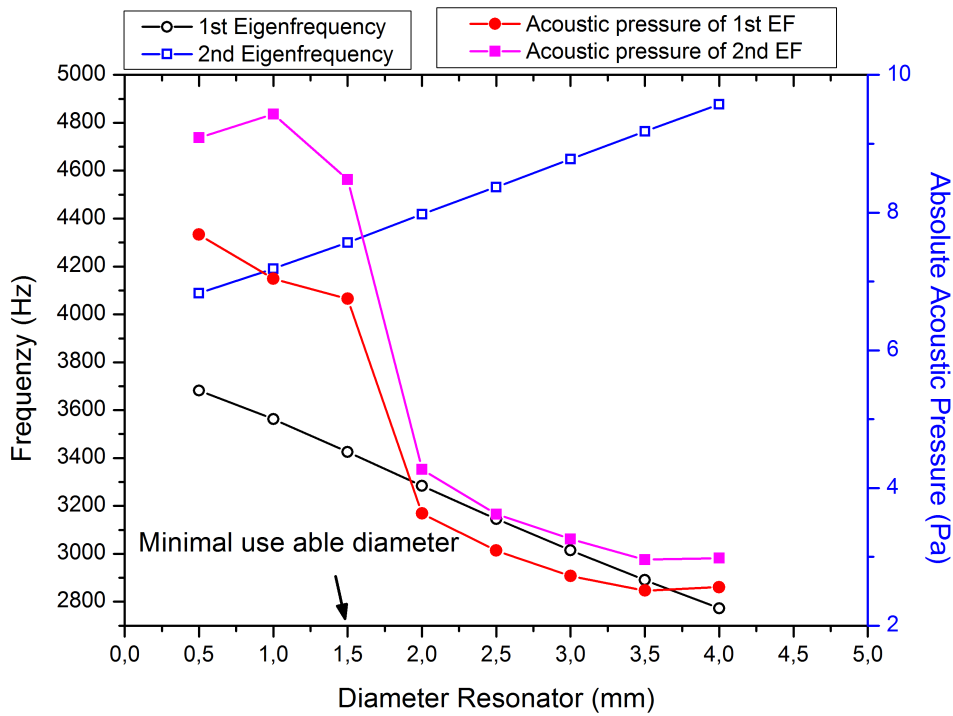


Figure 44: Frequency shift / pressure change in addition of the resonator diameter - simulation

6 Conclusion

The requirement to enhance the photoacoustic signal by a redesign of the resonator was realized by the new absorber-resonator-system. Due to a ratio of 2 to 1 regarding to the acoustic lengths of absorber to resonator a special phenomenon of the Eigenfrequency spectrum could be discovered. Unlike the well-known Helmholtz resonator this resonator system has no diminution at the absorber-resonator transition rather a trumpet transition will bring the produced acoustic pressure into the resonator. If the diameter of the resonator becomes smaller an overlap of two resonances could be generated. This overlap of the resonances will create a 2 to 2.5 times higher acoustic pressure from the photoacoustic effect than the Micro Soot Sensor cell will do. This has been shown with the simulations and confirmed by the experimental measurements.

The in the experiments detected frequency position of each resonance in the resonant cells is relatively comparable to the results of the numerical calculation. The shift in the Eigenfrequency spectra is caused by the different speeds of sound in different materials. In the simulation the material was dry air at room temperature and in the experiments a NO_2 sample gas was used. The acoustic surface and volume losses are also not taken into account in the calculations which have an influence on the resulting acoustic pressure. A shift of the first Eigenfrequency to higher frequencies and a shift of the second Eigenfrequency to lower frequencies, in a T-shaped resonator with a absorber to resonator ratio of 2:1, by a becoming smaller resonator diameter are the results of the simulation and the measurements. The becoming higher pressure at the end of the resonator is also an effect of that. The overlap of two resonances was only detected in the experiments because the numerical calculation of the problem was simplified and the resonance peaks show no peak broadening which is the origin of the overlap.

Both kinds of used prototypes have their advantages and disadvantages but for the verification of the acoustic behavior of a geometry the rapid prototyped cell is to be preferred because of the costs.

List of Figures

1	Experimental setup of the photophone of Alexander Graham Bell for the analysis of materials (e.g. selen) [1]. The light is irradiated over a mirror and a collecting lens, is modulated by a chopper wheel, collimated with a lens to split the light afterwards with a prism into the spectral colors and excite the specimen. The photoacoustic signal is detected by a stethoscope.	10
2	Principle sketch of absorption spectroscopy	13
3	Modulated monochromatic light is irradiated into a resonant cell. Soot particles are excited by the light and dissipate the produced heat to the surrounding atmosphere. An acoustic signal is generated that is amplified by a resonator.	14
4	Experimental setup of a photoacoustic measurement system. The irradiation of monochromatic light and the beam path through a resonant cavity system is shown.	14
5	Absorption cross-section of NO_2 [8]	15
6	Photoacoustic signal NO_2 in dependency of the wavelength measured with a Micro Soot Sensor [22].	16
7	Infrared spectra of combustion generated soot at different temperatures. The figure shows local absorption maxima of soot, an absorption edge of CO_2 and a broad absorption region of H_2O [27].	17
8	Formation of soot particles over the reaction time of a combustion [26]. . .	19
9	Picture of a Soot particle from a combustion generated aerosol taken with Transmission Electron Microscope (TEM). The soot particle sticks on a carbon substrate (broad black area on the right side of the picture). . . .	20
10	Picture of primary particles of a soot particle shown in figure 9 also taken with a transmission electron microscope (TEM). The primary particles could be characterized by their degree of graphitization [17] [19] [26]. . . .	21
11	Pressure field of longitudinal, azimuthal and radial oscillations. The arrows show from fields of low pressure to fields of high pressure.	25
12	Directions of propagation of a sound wave in a cylindrical resonator in a one dimensional view [13].	26
13	User interface for selecting <i>Space Dimension</i>	29

14	User interface for selecting <i>Physics</i>	30
15	User interface for selecting <i>Study</i>	30
16	User interface of <i>Model Builder</i>	30
17	Both ends open resonator limited by two volumes. These volumes simulate the endless room where a propagating sound wave in the resonator is reflected.	33
18	Terms of a T-shaped cell	36
19	Nomenclature of a resonator system with the the characterizing values the length of the absorber, the length of the resonator and the diameter of the resonator.	37
20	In- and outlet of the cell (blue) are defined as sound soft boundaries	40
21	Meshed geometry of the cell T-42-21-1.5. The mesh is built up by triangular and tetrahedral elements.	41
22	Absolute pressure of the first and second Eigenfrequency of the cell T-42-21-1.5 along the respective cylinder axis. (a) shows the pressure along the axis of the absorber and (b) along the axis of the resonator. The first 3 mm in (b) are a part of the absorber.	43
23	Absolute pressure of the first (a) and second (b) Eigenfrequency of the cell T-42-21-1.5 on the surface.	44
24	Absolute pressure of the first (a) and second (b) Eigenfrequency of the cell T-42-21-1.5. Displayed are the iso-surfaces of equal pressure in the cell. A difference of the pressure field at the crossover can be seen and compared with figure 22.	45
25	Stainless steel cell PT-42-21-x with the removed upper shell.	50
26	Rapid prototyped cell PT-42-21-x	51
27	Photoacoustic signal in a stainless steel and a plastic (humid and dry) cell	53
28	Principle sketch of the experimental setup for the determination of the frequency spectra of different photoacoustic cells.	55
29	Experimental setup for the determination of the frequency spectra of different photoacoustic cells.	55
30	Polyetheretherketon PEEK insert to make the resonator diameter smaller from 3 mm to 1.5 mm	57

31	Photoacoustic signal enhanced by PT-42-21-x with different resonator diameters x and the Micro Soot Sensor	59
32	Overlap of the first and second Eigenfrequency by a becoming smaller diameter in T-resonator with a absorber length of 42 mm and a resonator length of 21 mm.	60
33	Resonance spectra of T-resonator with a absorber length of 21 mm and a resonator length of 21 mm with different resonator diameters.	64
34	Resonance spectra of T-resonator with a absorber length of 21 mm and a resonator length of 42 mm with different resonator diameters.	64
35	Resonance spectra of T-resonator with a absorber length of 42 mm and a resonator length of 21 mm with different resonator diameters.	65
36	Resonance spectra of T-resonator with a absorber length of 42 mm, a resonator length of 21 mm, an absorber diameter of 4 mm and with different resonator diameters.	65
37	Resonance spectra of T-resonator with a absorber length of 63 mm and a resonator length of 21 mm with different resonator diameters.	66
38	Resonance spectra of T-resonator with a absorber length of 63 mm and a resonator length of 42 mm with different resonator diameters.	66
39	Resonance spectra of T-resonator with a absorber length of 84 mm and a resonator length of 21 mm with different resonator diameters.	67
40	Resonance spectra of T-resonator with a absorber length of 84 mm and a resonator length of 42 mm with different resonator diameters.	67
41	Results of experiments regarding the frequency shift of two T-resonators in addition of the resonator diameter. The absorber-resonator ratio is for both 2:1.	72
42	Results of simulation regarding the frequency shift of two T-resonators in addition of the resonator diameter. The absorber-resonator ratio is for both 2:1.	72
43	Frequency shift / pressure change in addition of the resonator diameter - experiment	73
44	Frequency shift / pressure change in addition of the resonator diameter - simulation	73

References

- [1] Alexander Graham Bell, "On the Production and Reproduction of Sound by Light: the Photophone.", American Journal of Science, Series 3. No. 20, 1880, pp. 305-324
- [2] Alexander Graham Bell, "Selenium and the Photophone" Nature 22, 500-503, 23 September 1880
- [3] John Tyndall, "Action of an Intermittent Beam of Radiant Heat upon Gaseous Matter.", Proceedings of the Royal Society of London. 31, 1881, S. 307317
- [4] M.L. Viengerov, "New method of gas analysis based on Tyndall-Roentgen optoacoustic effect", Dokl. Akad. SSSR 19, 678-690 (1938)
- [5] Kerr, E.L. and J.G. Atwood, "The Laser Illuminated Absorptivity Spectrophone: A method for Measurement of Weak Absorptivity in Gases at Laser Wavelengths.", Appl. Opt., 1968. 7: p.915
- [6] Kreuzer, L.B., "Ultralow Gas Concentration Infrared Absorption Spectroscopy", J. Appl. Phys., 1971. 42: p.2934-2942
- [7] Dewey, C.F., R.D. Kamm, and C.E. Hackett, "Acoustic Amplifier for Detection of Atmospheric Pollutants", Appl. Phys. Lett., 1973. 23: p.633-635
- [8] Bogumil et al. 2000, Proc. ERS-Envisat Symposium
- [9] R. Raspet, W.V. Slaton, W.P. Arnott, H. Moosmüller "Evaporation - Condensation Effects on Resonant Photoacoustics of Volatile Aerosols", Journal of Atmospheric and Oceanic Technology (May 2003) Vol.20
- [10] H. Saathoff, KH. Naumann, M. Schnaiter, W. Schock, E. Weingartner, U. Baltensperger, L. Kramer, Z. Bozóki, U. Poschl, R. Niessner, U. Schurath "Carbon mass determinations during the AIDA soot aerosol campaign 1999", Journal of Aerosol Science 34 1399-1420 (2003)

- [11] W. Schindler, C. Haisch, H.A. Beck, R. Niessner, E. Jacob, D. Rothe "A photoacoustic sensor system for time resolved quantification of diesel soot emissions", Society of Automotive Engineers SP SP-1862 (Emissions Measurement and Testing) (2004) 151-158
- [12] B. Baumann, B. Kost, H. Groninga, M. Wolff "Eigenmodes of Photoacoustic T-Cells", COMSOL Multiphysics User's Conference 2005 Frankfurt
- [13] R. Lerch, G.M. Sessler, D. Wolf "Technische Akustik - Grundlagen und Anwendungen", Springer Verlag e-ISBN 978-3-540-49833-9
- [14] M. Möser "Technische AKustik", Springer Verlag e-ISBN 978-3-540-89817-7
- [15] Harald A. Beck "Anwendung der Photoakustischen Spektroskopie in der Prozess - und Umweltanalytik", Dissertation (2003), Fakultät für Chemie, Technische Universität München
- [16] Thomas Rück "Aufbau eines Messplatzes zur Photoakustischen Detektion von NO_2 und Einflussnahme physikalischer Parameter", Diplomarbeit (2010) Naturwissenschaftliche Fakultät IV - Chemie und Pharmazie - Universität Regensburg
- [17] Tristan Reinisch "Über die Morphologie von Russpartikel von Verbrennungskraftmotoren im Hinblick auf Partikelanzahlmessung", Bachelorarbeit (2010) Institut für Elektronenmikroskopie und Feinstrukturforschung - Technische universität Graz
- [18] A. Elia "Qantum cascade laser-based photoacoustic spectroscopy of volatile chemicals: Application to hexamethyldisilazane", Spectrochimica Acta Part A 64 (2006) 426-429
- [19] Stefan Kamm "Kinetische Untersuchungen der Oxidation von luftgetragenen Rußpartikeln mittels ESR- und FTIR-Spektroskopie", Dissertation (2000) Naturwissenschaftlich-Mathematische Gesamtfakultät der Ruprecht-Karls-Universität Heidelberg

- [20] H. Helmholtz "Theorie der Luftschwingungen in Röhren mit offenen Enden" Journal für die reine und angewandte Mathematik, Bd. LVII, S.1-72. Berlin 1860
- [21] Pratsinis S.E. et al. "The Structure of Agglomerates Consisting of Polydisperse Nanoparticles", 16th ETH Conference on Combustion Generated Particles
- [22] Tristan Reinisch, Alexander Bergmann, Robert Diewald, Michael Arndt, Bernhard Gaulhofer, Roland Resel "Approaches to reduce the cross-sensitivity in photoacoustic soot measuring", 16th ETH Conference on Combustion Generated Particles
- [23] <http://www.ift.tugraz.at/rapidprototyping/index.php>, retrieved at 24.August 2012 12:55
- [24] "COMSOL Multiphysics User's Guide", Comsol 4.0a June 2010
- [25] Thomas Huemer "Automatische Vernetzung und adaptive nichtlineare statische Berechnung von Flächentragwerken mittel vierknotiger finiter Elemente", Dissertation an der Technischen Universität Wien, 1999
- [26] S. Hausberger "Schadstoffbildung und Emissionsminimierung bei Kfz - Abgasnachbehandlung", Vorlesungsunterlagen der Lehrveranstaltung Nr.313 180 an der Technischen Universität Graz, 20.12.2010
- [27] Yuki Kimura et al. "Production and structural characterization of carbon soot with narrow UV absorption feature", Carbon 42 (2004) 33-38